UC San Diego

UC San Diego Electronic Theses and Dissertations

Title

The growth of Nacre in Abalone : seasonal and feeding effects on the process of mineral formation

Permalink

https://escholarship.org/uc/item/15j0q3bn

Author

López, Maria Isabel

Publication Date

2011

Peer reviewed|Thesis/dissertation

eScholarship.org Powered by the California Digital Library
University of California

UNIVERSITY OF CALIFORNIA, SAN DIEGO

The Growth of Nacre in Abalone: Seasonal and Feeding Effects on the Process of Mineral Formation

A Thesis submitted in partial satisfaction of the requirements for the degree of

Master of Science

in

Materials Science and Engineering

by

Maria Isabel López

Committee in charge:

Professor Marc André Meyers, Chair
Professor Joanna McKittrick
Professor Jan B. Talbot

2011

The Thesis of Maria Isabel Lopez is approved and it is acceptable in quality and form for publication on microfilm and electronically:

Chair

University of California, San Diego

2011

“Un buen padre vale por cien maestros.”

- Jean Jaques Rosseau

Dedicado con amor a mis padres.

'The most exciting phrase to hear in science,

the one that heralds new discoveries,

is not "Eureka!" ("I found it!") but rather

"hmm....that's funny..."'

- Isaac Asimov

TABLE OF CONTENTS

Signature page……..... iii

Dedication…… iv

Epigraph ……..…… v

Table of contents…….. vi

List of figures……..…….. viii

List of tables……. xii

Acknowledgements…….. xiii

Vita……...…… xv

Abstract……...……. xvi

Chapter 1 introduction and objectives……...……... 1

Chapter 2 background……..... 10

2.1Structure and mechanical properties……...…… 10

2.1.1Structure of abalone shell and abalone nacre……..……. 10

2.1.2 Mechanical behavior of nacre: early work…….. 17

2.1.3 Compression studies of abalone nacre……...…….…… 17

2.1.4 Tension studies of abalone nacre……..……..…… 19

2.1.5 Structure and property relationship……. 24

2.2 Growth and Biomineralization .....……...…… 38

Chapter 3 experimental methods……. 46

3.1 Culturing facilities……...…...……...…. 46

3.2 Specimen collection, preparation, and characterization……. 48

3.2.1 Flat pearl……..…..… 48

3.2.2 Demineralization of nacre……..…..… 49

3.2.3 Structural characterization of epithelium…… 50

3.2.4 Scanning electron microscopy observations on the structure of nacre…….. 52

3.2.5 Atomic force microscopy……..……. 55

3.2.6 Critical point drying……..……..... 56

Chapter 4 results and discussion……..…..…….. 57

4.1 Characterization of growth surfaces……..... 57

4.2 Epithelium observations……..…….…….. 69

4.3 Demineralized shell and organic interlayer……..…….. 73

Chapter 5 Summary and Conclusions……..... 81

References……..……... 86

LIST OF FIGURES

Figure 1.1: Schematic representation of contributing scientific fields ……..… 1

Figure 1.2: Schematic representation of characteristic constraints/components in the study of biological systems. (*source*: Meyers et al. 2010) …..……. 6

Figure 2.1: Structure of typical mollusk shell …… 11

Figure 2.2: Comparison of the calcite and aragonite unit cells. (a) top view of calcite, (b) tridimensional view of calcite unit cell, (c) top view of aragonite, (d)tridimensional view of aragonite unit cell. Note that the large spheres depict the calcium ions, the small darker spheres depict the oxygen ions, and the smaller lighter spheres show the carbon ions ……..… 12

Figure 2.3: Abalone mantle pushed back revealing epithelium ……..….... 13

Figure 2.4: The levels of structural hierarchy in nacre; macro scale mesolayers, 10μm by 0.5 μm aragonite tiles, the nanostructure defined within the interface between tiles ……..... 14

Figure 2.5: Hierarchical structure (5 levels) of the abalone nacre from nano-, micro-, to meso- to structural length scales. (*source*: Meyers et al. 2010) …… 16

Figure 2.6: Compressive strength of freshly sectioned nacre perpendicular to layered structure (*source*: Lin 2008b) ……...…… 19

Figure 2.7: Weibull distribution of tensile strength perpendicular to layered structure (*source*: Lin 2008b) ….……... 20

Figure 2.8: Weibull distribution of tensile loading parallel to layered structure (*source*: Lin 2008b) ……..……. 22

Figure 2.9: Strength of nacre with respect to loading direction, parallel lines represent growth bands (*source*: Lin 2008b) ……. 23

Figure 2.10: Organic layer acting as a viscoelastic glue (*source*: Lin 2008b)….. 26

Figure 2.11: Principal mechanisms of damage accumulation in shells: (a) viscoplastic deformation of organic layers; (b) crack deflection by organic layers; (c) delocalization of damage (*source*: Menig et al. 2000) ……..…….. 27

Figure 2.12: Side view of intermediate tile growth through organic layers on flat pearl five weeks after implantation (*source*: Lin 2008b) ……... 28

Figure 2.13: Schematic showing terraced growth and organic membrane sagging under its own weight (*source*: Lin 2008b) ……..…….. 28

Figure 2.14: Calculated (a) stress, and (b) elastic modulus of organic layer as a function of deflection for two circle radii (assumed shape between sagging points of the membrane) are considered: 2.5 and 5 μm (Source: Lin, 2008b) ….... 29

Figure 2.15: Asperities, many of which are remnants of mineral bridges, concentrated at the center of an aragonite tile after 9 hours of deproteination (*source*: Lin 2008b) ……..…. 30

Figure 2.16: Mineral bridges (marked by arrows) between aragonite tiles after 9 hours of deproteination (*source*: Lin 2008b) ……...…….... 31

Figure 2.17: Transmission electron micrograph of nacre crossection showing mineral bridges between tile interfaces (*source*: Lin 2008b) ……. 32

Figure 2.18: Mineral bridges (marked by arrows) between tile layers (*source*: Lin 2008b)…… 32

Figure 2.19: Origin of toughening in nacre: (a) SEM micrograph showing sliding of tiles in tensile loading; (b) balance between tile fracture and intertile shear; (c) details of three mechanisms of intertile shear: asperities, organic layer acting as viscoelastic glue, and fracture of mineral bridges. (*source*: Meyers et al. 2010) ……..... 34

Figure 2.20: Strength and toughness as a function of number of hierarchical levels. (*source*: Meyers et al. 2010) ……..…..….. 36

Figure 2.21: SEM micrograph showing interlocks in nacre. Schematic representing the mismatch in layering giving rise to interlocks (*source*: Katti & Katti 2006)……..... 37

Figure 2.22: (a) Macrostructural view of a cross section of the *Haliotis rufescens* shell. Growth bands are observed separating larger regions of nacre, (b) SEM micrograph of fracture surface; direction of growth marked with arrow (*source*: Lin 2008a) ……..…….. 39

Figure 2.23: Order of events during mesolayer growth in nacre (*source*: Lin 2008a)..... 40

Figure 2.24: Summary of sequential growth from flat pearl and trepanning experiments (*source*: Lin 2008a) ……..….... 42

Figure 2.25: Transmission electron microscopy of tiled aragonite nacre with selected area diffraction (*source*: Lin 2008b) ……..…….……...…… 43

Figure 2.26: Schematic of the forces acting on the growth surface of the shell (*source*: Lin 2008b) ……..……..……..…… 44

Figure 3.1: Abalone culturing facilities (a) Large open water tank and (b) 45 liter open water fish tank at the Scripps Institution of Oceanography ……..... 47

Figure 3.2: Glass slides (depicted by arrows) embedded in abalone shell ..……... 49

Figure 3.3: Completely demineralized abalone nacre. Separation of layer occurs as the mineral is removed and the material looses most of its structural integrity.. 50

Figure 3.4: Abalone mantle pushed back revealing epithelium (depicted by arrow) prior to excision ……...…… 51

Figure 3.5: (a) Basic components and the control console of SEM, (b) the detail in the chamber of SEM (*source*: Goldestein et al. 2003) …….. 53

Figure 3.6: Scanning Electron Facility at Calit2 at UCSD …… 54

Figure 3.7: Schematic diagram of Atomic Force Microscope ……... 56

Figure 4.1: Sequential growth results 1 week after implantation. a) Growth at 21°C with abalone regularly fed; b) Growth at 15°C with abalone regularly fed; c) Growth at 20°C without food available ……. 59

Figure 4.2: Sequential growth results 1 week after implantation. a) Growth at 21° C with abalone regularly fed showing the coverage exhibited by the tiles (top view); b) higher resolution of top view of growth at 21° C with abalone regularly fed (top view); c) Growth at 20° C without food available …… 60

Figure 4.3: Sequential growth results 2 weeks after implantation. a) Cross-sectional view of growth at 21°C with abalone regularly fed; b) Growth at 15°C with abalone regularly fed; c) Growth at 20°C without feeding ……..…….. 62

Figure 4.4: Sequential growth results after 3 weeks of implantation. a) Growth at 21°C with abalone regularly fed (cross-section); b) Detailed view of aragonite tile morphology; c) Growth in 15°C with abalone regularly fed; d) Growth in 20°C without food available ……..….. 65

Figure 4.5: Atomic force microscopy of growth surface in 21°C showing the aragonite tile growth. a) Top view; b) Tridimensional view …….. 67

Figure 4.6: Atomic force microscopy of growth surface in 15°C showing the columnar structure. a) Top view; b) Tridimensional view ……...…….. 68

Figure 4.7: a) Sectioned epithelium; surface in contact with growing edge of shell depicting flat outer surface (I) and area where surface was scraped off (II); b) Detailed view of flat outer surface of epithelium. c) Array of channels within epithelium (channels depicted by arrows); d) Fibrils within channels (marked with arrows) ……..……..… 70

Figure 4.8: Schematic depicting hypothetical mechanism by which epithelium generates chitin fibrils and 'squeezes' them onto growth surface ……. 71

Figure 4.9: Microvilli depictions in nacre. (a) TEM of section of nacre from *Pinctada radiate*. Note the visible microvilli at the edge of the mantle epithelium (M) and extrapallial space (X). (b) Schematic illustration of nacre formation in gastropods. Aragonite tablets (A); Organic sheets (S); surface sheet (SS); Organic envelope surrounding crystals (E); Newly formed crystals (N); and part of epithelium (M) and extrapallial space (X). (*source*: Nakahara 1991) ……..... 72

Figure 4.10: Schematic depiction of the epithelium cells containing the microvilli which are approximately 100 nm diameter and 400 nm height which involves in the deposition and position of the organic membrane …… 73

Figure 4.11: Demineralized shell revealing randomly oriented chitin fibrils from intertile layers; b) schematic representation of organic intertile layer composed of chitin fibrils. c) Schematic structure of chitin ……..……..... 76

Figure 4.12: Thin intertile organic layer showing holes; b) Proposed Mechanism of growth of nacreous tiles by formation of mineral bridges as depicted by Meyers et al. (Meyers et al. 2009); organic layer is permeable to calcium and carbonate ions which nourish lateral growth as periodic secretion and deposition of the organic intertile membranes restricts their flux to the lateral growth surfaces. Arrows A designate organic interlayer imaged by SEM; arrow B designates lateral boundary of tile ……..……... 77

Figure 4.13: (a) Growth sequence through mineral bridges (b) Detailed view of mineral bridges forming through holes in organic membranes (*source*: Lin 2008b) ……..……... 79

Figure: 5.1: Microstructure of abalone nacre-inspired Al_2O_3/PMMA composites in (a) lamellar and (b) brick-and-mortar forms produced by freeze casting techniques; (c) bridge between two tile layers (*source*: Launey et al. 2009) …..… 84

LIST OF TABLES:

Table 1.1: Principal components of biological materials (*source*: Meyers et al. 2010) ……... 3

Table 3.1: Experimental conditions; temperature and dietary condition …….. 48

ACKNOWLEDGEMENTS

I would like to thank all of the members of the Marc Meyers' and Joanna McKittrick's group for their continuous support, in particular Po-Yu Chen who largely contributed to this work both in content, mentorship, friendship, and in motivation. In addition Chung-Ting Wei and Yen-Shan Lin for their help in introducing me to the lab and their constant help with troubleshooting when problems arise. My close friends and my boyfriend are also acknowledged, as they at different times in my career have provided aid, patience, and support.

Ryan Anderson's and Maribel Montero's assistance at Calit2 facility at UCSD are greatly acknowledged. Eddie Kisfaludy's and Aruni Suwarnasarn's expertise at the Laboratory facilities at the Scripps Institution of Oceanography are also greatly appreciated. I would also like to thank Professor Jan B. Talbot for her insightful observations and professional opinion.

I would like to give a special thanks to Professor Joanna McKittrick for her constant support, mentorship, insight, and encouragement. Professor Marc A. Meyers, who provided extensive mentorship and support over the last two years, will always be acknowledged as a major impact in my understanding of research and academia.

Finally, I would like to give an extended thanks to my parents who have laid the groundwork for my academic accomplishments and who continuously inspire, support and motivate me.

This research is supported by the National Science Foundation, Division of Materials Research, Ceramics Program (DMR1006931) and by a National Research Council & Ford Foundation Predoctoral Fellowship.

Chapter 4, in part, is a reprint of the material as it appears in Lopez MI, Chen PY, McKittrick J, Meyers MA. *Materials Science and Engineering C* 2010; 31: 238-245. The thesis author was the primary investigator and author of this paper.

VITA

6/2009-6/2011 Materials Science and Engineering Program, University of California, San Diego. M.S. in Materials Science, (AGEP and Ford Foundation Fellow).
6/2005-5/2009 Metallurgy and Materials Engineering, The University of Texas at El Paso. B.S. in Metallurgy and Materials Engineering. 2009.

FIELD OF STUDY

Major: Materials science and engineering with an emphasis on the study of biological materials.

ABSTRACT OF THE THESIS

The Growth of Nacre in Abalone: Seasonal and Feeding Effects on the Process of Mineral Formation

by

Maria Isabel López

Master of Science in Materials Science and Engineering

University of California, at San Diego, 2008

Professor Marc André Meyers, Chair

The processes of aggregation of mineral and organic materials to the growing surfaces in red abalone (*Haliotis rufescens*) are analyzed. The flat pearl implantation method is used to observe the transient stages of calcium carbonate deposition, the structure of the organic interlayer, and the steady-state growth of aragonite tiles. The morphology of the organic interlayer and the epithelium region are characterized by scanning electron microscopy. These results enable a realistic depiction of the formation of the terraced cones that comprise the principal biomineralization mechanism in this gastropod. The transition rate was compared in a normally fed and in a starved gastropod and found to be higher in the former. The effect of water temperature (or seasonal) was also established, growth proceeding faster in the summer (T~ 21°C) than in winter at 15°C.

CHAPTER 1

INTRODUCTION AND OBJECTIVES

Material Science and Engineering is an interdisciplinary field that has been generally known to incorporate elements of applied physics and chemistry. It has expanded into three main directions: metals, polymers, and ceramics. However, with the emerging interest in biomimetics (human-made processes, substances, devices, or systems that imitate nature, biology has played an important role (Figure 1.1), opening a whole other perspective of material science.

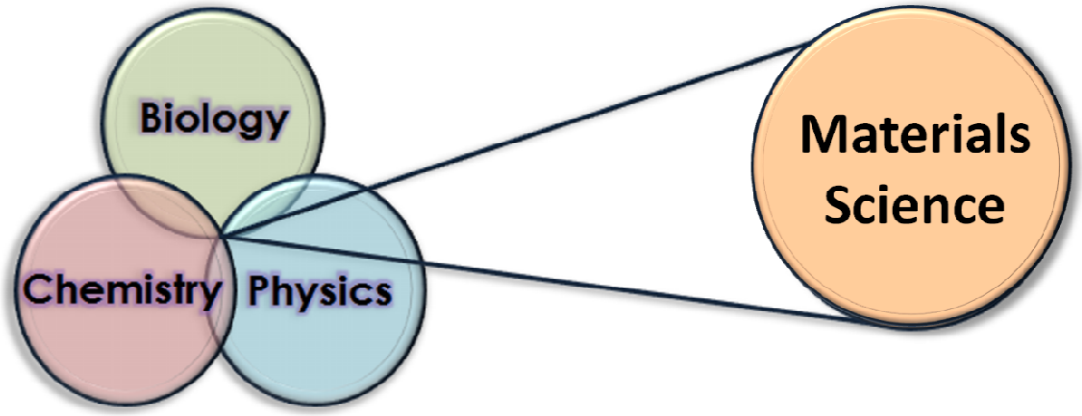

Figure 1.1: Schematic representation of contributing scientific fields

Nature can provide excellent solutions to many engineering problems. Biological organisms are improved and refined by natural selection. Natural selection holds many teachings from which scientists and engineers can learn and understand which may lead to novel, better ways of designing and processing materials. 'Biomimicry', or 'Biomimetics', is a alluring new field that introduces the idea of

understanding the property and structure relationship of biological materials in hopes of developing novel means of designing and processing materials. This field interties well the disciplines of materials science and biology in an effort to solve complex multidisciplinary scientific problems. This effort was first pioneered by D'Arcy W. Thompson as early as 1917 (Thompson 1968) followed by other well known works such as Vincent (Vincent 1991) and Currey (Currey 2002).

Biological Material Science is composed of three main areas defined as follows:

- Biological materials: natural materials.
- Bioinspired/ biomimicked materials: bioinspired materials and design.
- Biomaterials: synthetic materials in biomedical applications.

These three main areas are many times mutually dependent and interconnected.

It is important to highlight that in this new emerging field a clear understanding of biology is important. Animal anatomy, physiology, and lifestyle are important as they many times determine the development and behavior of the structural parts. Therefore it is imperative for material scientists to understand these biological, or natural, materials. This is analogous, for example, in how a materials scientist must understand the engineering structures in their materials used when working on engineering projects. Table 1.1 shows the principal components of biological materials. They can be divided into two groups: organic materials and biominerals. Organic materials that can be likened to polymers in materials science and engineering, they provide a greater ability to undergo deformation, whereas the

minerals sustain loading. The organic components can be extended in tension, whereas the ceramic resists primarily compression. Therefore the minerals primarily add the stiffness and strength while the biopolymers add toughness and ductility.

Table 1.1: Principal components of biological materials (Source: Meyers et al. 2010).

Table 1 – Principal components of biological materials.

Hard component: minerals	Soft component: organic macromolecules
Calcium carbonate ($CaCO_3$)	Collagen (Types I, II,. . . , XXVIII)
Calcium phosphate (hydroxyapatite, $Ca_{10}(PO_4)_6(OH)_2$)	Keratin
Silica (SiO_2)	Chitin
Magnetite (Fe_3O_4)	Elastin
Copper oxide	Cellulose
	Resilin and Abductin

Many biological systems have excellent mechanical properties not yet achieved by synthetic materials (Currey 2002; Arzt 2006) even though the basic polymers and minerals used in natural systems are quite weak, e.g. calcium carbonate alone is quite brittle. Nonetheless, when these inorganic components are combined with proteins in a highly ordered structure they form very strong composites. These refined, highly ordered, self-assembled structures can enhance their mechanical properties, such as increasing their strength, by orders of magnitude (Vincent 1991; Zhang 2002). These systems are subject to complex constraints that exhibit specific characteristics presented in the hexagon shown in Figure 1.2 (source: Meyers et al. 2010). Biological materials are unique in their conception, design, and structure. The six components of the hexagon are self assembly, hierarchy of structure, functionality, ambient temperature and pressure processing, evolution/environmental constraints, and the importance of hydration to its structure and properties. These unique characteristics distinguish them from synthetic counterparts. The six components are presented below:

- The structures are assembled from the bottom-up, rather than from the top-down. This is a necessity of the growth process, since there is no availability of an overriding scaffold. This characteristic is called ‘self-assembly’.
- Many components serve more than one purpose, a characteristic refined by over a billion years of evolution. Thus, the structures are called “multifunctional’.
- The properties are highly dependent on the level of water in the structure.

- Evolution, environmental constraints, and the limited availability of materials dictate the morphology and properties. The principal elements available are oxygen, nitrogen, hydrogen, calcium, phosphorous, silicon, sulfur, and carbon. The most useful synthetic metals (iron, aluminum, copper) are virtually absent and are only present in minute quantities and highly specialized applications. The processing of these elements requires high temperature processes not available in natural organisms.
- For the most part the synthesis of biological materials is conducted in an aqueous environment at ambient temperature and pressure of 1 atm.
- The structures are hierarchical, i.e., they have different scale levels conferring distinct properties. Biological systems are organized based on composition and structure, exhibiting a hierarchical organization from the nano, micro, to the macro (structural) level.

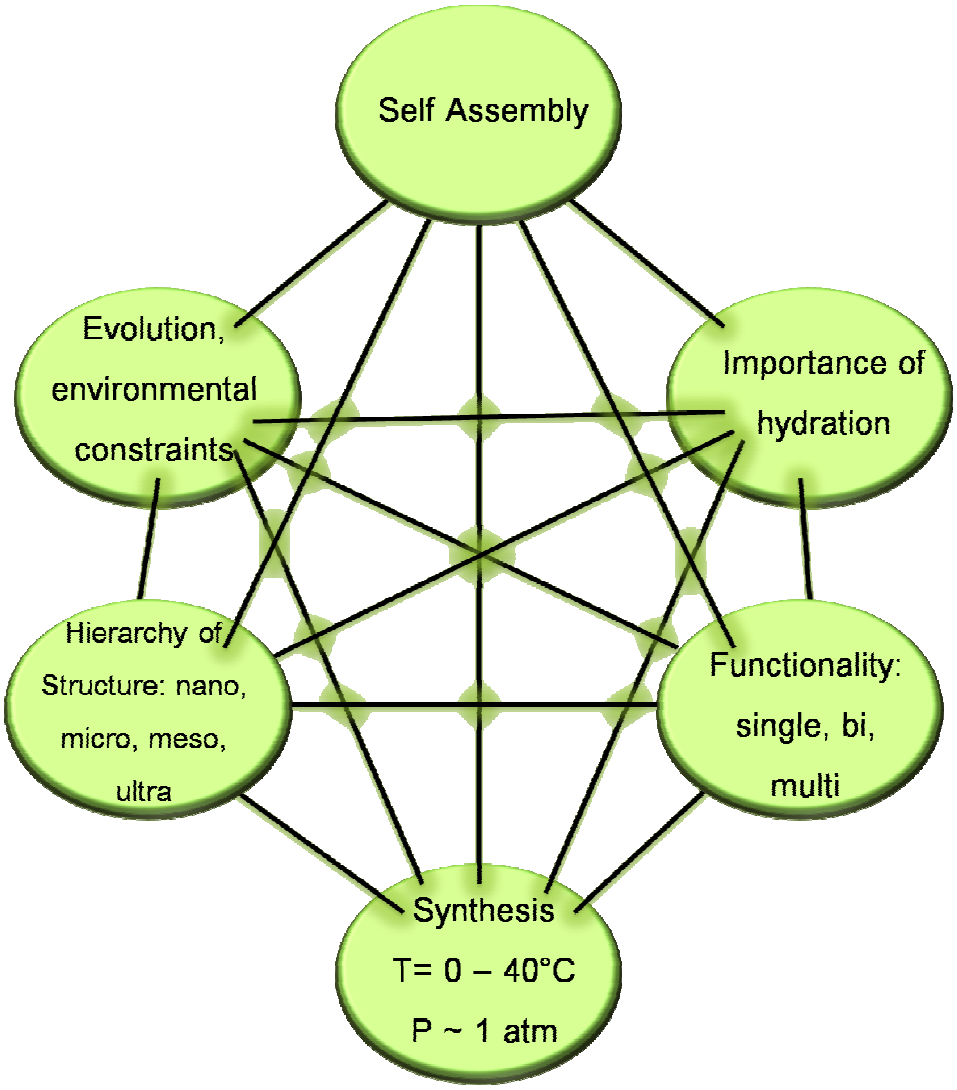

Figure 1.2: Schematic representation of characteristic constraints/components in the study of biological systems. (Source: Meyers et al. 2010)

Understanding the process in which living organisms control the growth of structured inorganic materials can inspire new and better synthetic materials (Sarikaya 1994; Srinivasan 1991; Mayer 2002, 2005; Sanchez 2005). Mollusk shells are a particular case of mineralized materials and have been intensively studied as biomineralization models (Luz and Mano 2009). Shells are of interest as so many different morphological types of shell structures can be found. According to Kobayashi & Samata 2006 in bivalve shells it is possible to differentiate from ten different morphologies, including: simple prismatic, aragonite prismatic, nacreous, foliated, composite prismatic, crossed lamellar structure, complex crossed lamellar or homogeneous structure. It is accepted that such structures can be associated with the excellent mechanical properties, especially when referring to the case of abalone nacre. Biomimetic strategies have been proposed to produce new layered composites resembling the structure of nacre. There have been recent successes in synthesizing a ceramic/polymer composite with outstanding toughness inspired by the structure of nacre in the abalone shell (Launey 2009, Munch 2008, Deville 2006 a,b), these results will be further discussed in Chapter 2.

Furthermore, the growth of nacre is a well studied subject characterized by many researchers (Meyers 2008, 2009, 2010; Bevelander 1980, 1982; Wada 1972; Nakahara 1979, 1982, 1991; Lin 2005, 2008; Mutvei 1980; Fritz 1994, 1998; Belcher 1996, 1997, 2000; Shen 1997; Schäffer 1996; Zaremba 1996; Sarikaya 1990, 1992; Espinosa 2009; Checa 2009; Bezares 2008, 2010). In particular, the growth and structure relationship has been studied in detail (Meyers 2008; Fritz 1994, 1998; Belcher 1996, 2000; Lin 2008). Results show that aragonite crystals first radiate from

nucleation sites forming a spherulitic pattern, then, columnar aragonite crystals form preferentially in the *c* direction (perpendicular to the growth surface). This morphology is then replaced by the aragonite tile pattern. Lin et al. (Lin 2008) examined the structure during a period of 1 to 6 weeks. In the third week, the columnar growth still dominated and by the sixth week terraced cones of the aragonite nacre became present.

Moreover, the role of the organic layer in the growth of the abalone nacre has been studied by Belcher et al. (Belcher 1996, 1997, 2000), Zaremba et al. (Zaremba 1996), Sarikaya et al. (Sarikaya 1990, 1992, 1994), Lin et al. (Lin 2005, 2008), Meyers et al. (Meyers 2008, 2009), and Bezares et al. (Bezares 2008, 2010), which has led to proposed mechanisms of growth (a further in-depth discussion of past growth observations will be given in Chapter 2). However, little attention has been paid to factors that affect the development of these transient phases.

Changes in the feeding patterns may limit the source of ions for mineral formation in the abalone shell. In addition, changes in its environment, such as temperature of the sea water, might affect the nucleation rate and growth rate of the transitory phases of calcium carbonate. Thus, the environment may play an important role in the mineral formation. Additionally, past studies suggest a large involvement of the mantle and epithelial cell layer to form the intricate structure of the growing front of the shell. For example, calcium radioisotopes movement studies on the oyster *Crassostrea virginica* show that movement of the ^{45}Ca out of the mantle correlated with the amount of ^{45}Ca deposited on the shell growth front. Additional mollusk ion

transport studies on the isolated mantle indicate ion movements from the mantle to the shell, while other studies suggest that Ca^{2+} transport occurs by diffusion through this mantle (Simkiss 1989). However, this process is not fully understood and studies of this soft tissue can give insights into this biomineralization process.

This study intends to investigate the process of mineralization following periods of growth interruption, taking into consideration important environmental factors (access to food and temperature) and to employ high-magnification characterization techniques to better understand how the soft tissue (e.g. epithelium and organic membrane) influences the mechanism of growth. These results are significant to the understanding the important characteristics of abalone nacre, such as the structure and mechanical properties, and an aid in improving the latest attempts to produce novel nacre-inspired materials.

CHAPTER 2

BACKGROUND

A combined background of past, relevant, and fundamental works will be described in this chapter in attempt of providing basic information pertaining to this study. The background will be divided into two main components: the structure and mechanical properties of the shell and shell growth and development studies. These two topics will hopefully cover the most relevant information pertaining to the present study and will allow for a better understanding of the latest results.

2.1 Structure & Mechanical Properties

2.1.1 Structure of Abalone Shell and Abalone Nacre

The abalone shell serves primarily as a protection method against predators. It surrounds the abalone body limiting the exposed area. Figure 2.1 is a schematic showing the shell is composed of two distinct layers: an outer prismatic layer (rhombohedral calcite) Figure 2.2 a, b and an inner nacreous layer (orthorhombic aragonite) Figure 2.2 c, d (Nakahara et al. 1982). The outer layer (calcite) is hard and brittle, and the inner layer (nacre) is a tough and ductile material. Lately, the outside calcite layer has received special attention, for example work reported by Heiland et al. (Heiland et al. 2011) has shown interesting results and beautiful images of this component. However, the inner nacreous layer is what mostly influences the mechanical response of the shell, thus it has become an interesting area of study and the focus of this work.

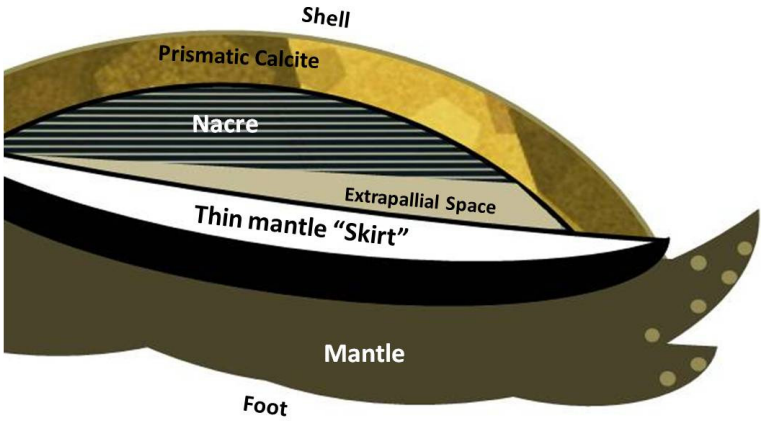

Figure 2.1: Structure of typical mollusk shell

It is also important to pay attention to other areas of the abalone beyond the shell. Figure 2.3 shows that when the growing surface of the shell ends it directly encounters the foot. The very small free space between the shell and the foot is called the extrapallial space, where the growth takes place. In this intersection there are important anatomical elements to consider. The epipodium, a sensory area which has tentacles, circles the foot and lies underneath the mantle. The mantle, also commonly referred as the epithelium (Figure 2.3), is in direct contact with the growing surface of the shell and thus is considered as an important factor in the growth mechanism.

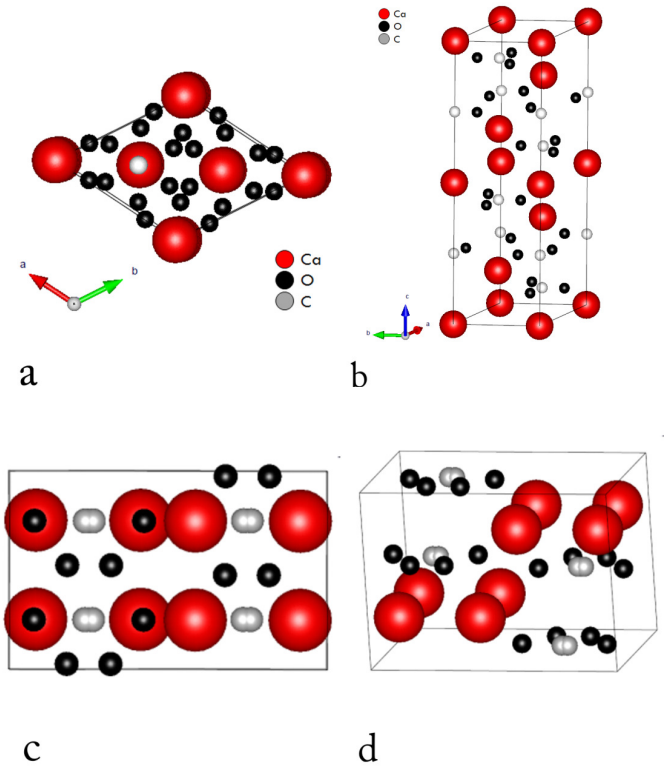

Figure 2.2: Comparison of the calcite and aragonite unit cells. (a) top view of calcite, (b) tridimensional view of calcite unit cell, (c) top view of aragonite, (d) tridimensional view of aragonite unit cell. Note that the large spheres depict the calcium ions, the small darker spheres depict the oxygen ions, and the smaller lighter spheres show the carbon ions.

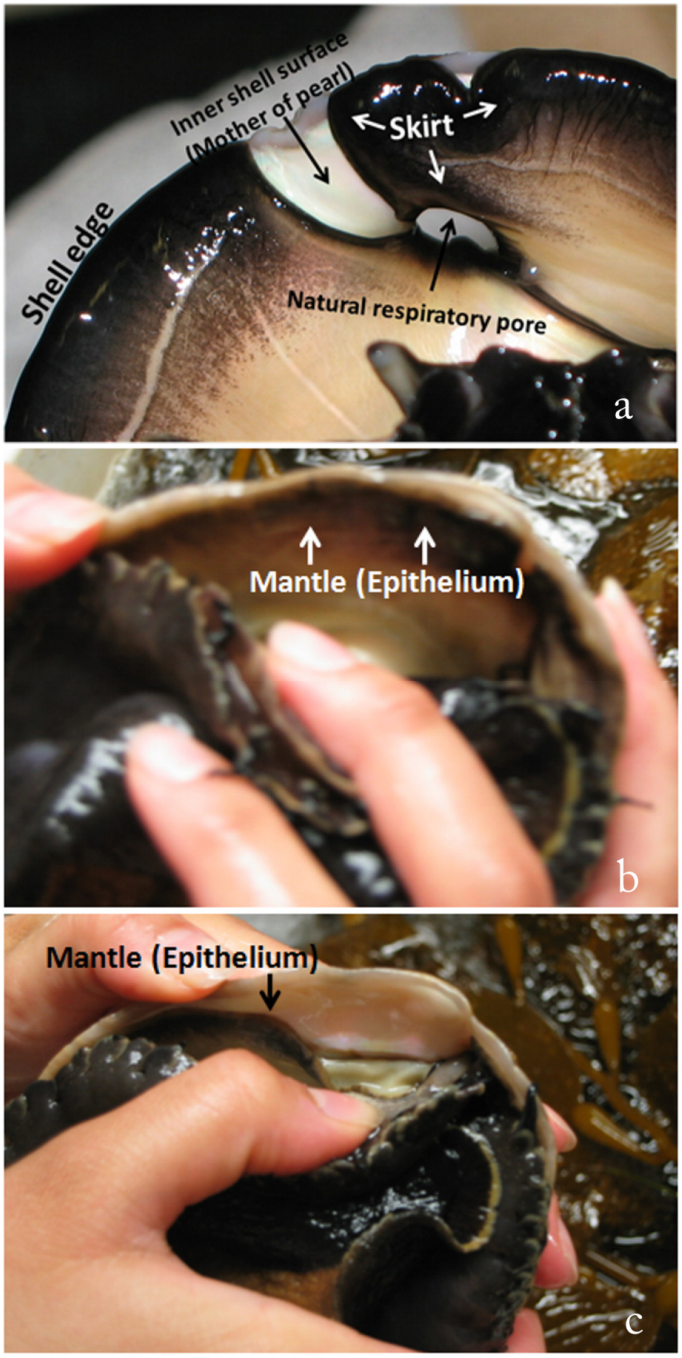

Figure 2.3: Abalone mantle pushed back revealing epithelium.

The abalone shell exhibits, as many other biological materials, various levels of hierarchy (Figure 2.4). First, the nacreous portion is composed of mesolayers ~0.3 mm thick, separated by organic layers embedded with calcium carbonate (Meyers et al., 2008a, b). These mesolayers are thought to be the result of seasonal growth bands (Figure 2.4). The darker regions are composed of inorganic component believed to be deposited by the animal in periods Furthermore, the inner nacreous layer is a ceramic/ organic composite (95 wt% ceramic, 5 wt% organic material) made up of nanoscale platelets of aragonite (a $CaCO_3$ polymorph) separated by an intertile matrix of organic biopolymers, described as "brick-and mortar" structure (Sarikaya 1994).

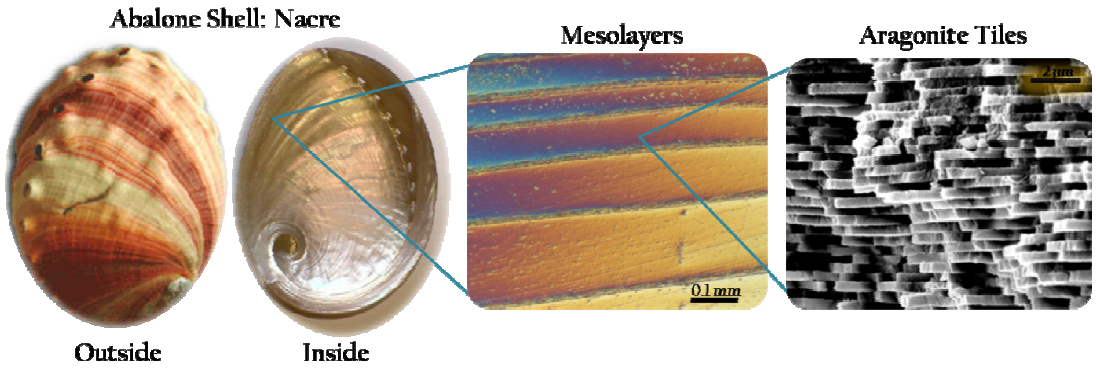

Figure 2.4: The levels of structural hierarchy in nacre; macro scale mesolayers, 10µm by 0.5 µm aragonite tiles, the nanostructure defined within the interface between tiles.

The platelets or tiles are 0.5 µm thick and 10 µm wide and the intertile layer is approximately 20 to 50 nm thick (Figure 2.4). (Menig et al. 2000; Lin and Meyers 2005; Lin et al. 2006, 2007; Meyers et al. 2008b) and others (Watanabe and Wilber 1960; Wada 1964; Towe and Hamilton 1968; Bevelander and Nakahara 1970; Erben 1972; Sarikaya and Aksay 1992; Fritz et al. 1994; Manne et al. 1994; Falini et al.

1996; Zaremba et al. 1996; Schäffer et al. 1997; Addadi et al. 2006). This highly ordered structure results in outstanding mechanical properties. Furthermore, the abalone shell's organized structure extends to the nanoscale. There are five different levels identified (Figure 2.5; *source*: Meyers et al. 2010):

- Level I is the molecular structure of the chitin fibers that are the structural component of the intertile organic layers and of the atomic crystalline structure of the aragonite.
- Level II is composed of the mineral bridges between tiles, with a diameter of 20-50 nm; it also comprises the sandwich structure of the organic intertile layer, with a core consisting of a random dispersion of chitin fibrils and a thickness equal to the length of the mineral bridges (~20 nm). The tiles may also be comprised by nanosize islands.
- Level III are the well recognized hexagonal tiles, with lateral dimensions of 10 μm and thickness of 0.5 μm.
- Level IV are the mesolayers, which are formed by seasonal fluctuations and are characterized by a thick organic layer (thickness ~200 μm) separating tile assemblages with approximately 0.1 -0.3 mm.
- Level V is the entire structure that, because of its architecture (dome shape, thickness distribution, etc) is optimized for strength and toughness.

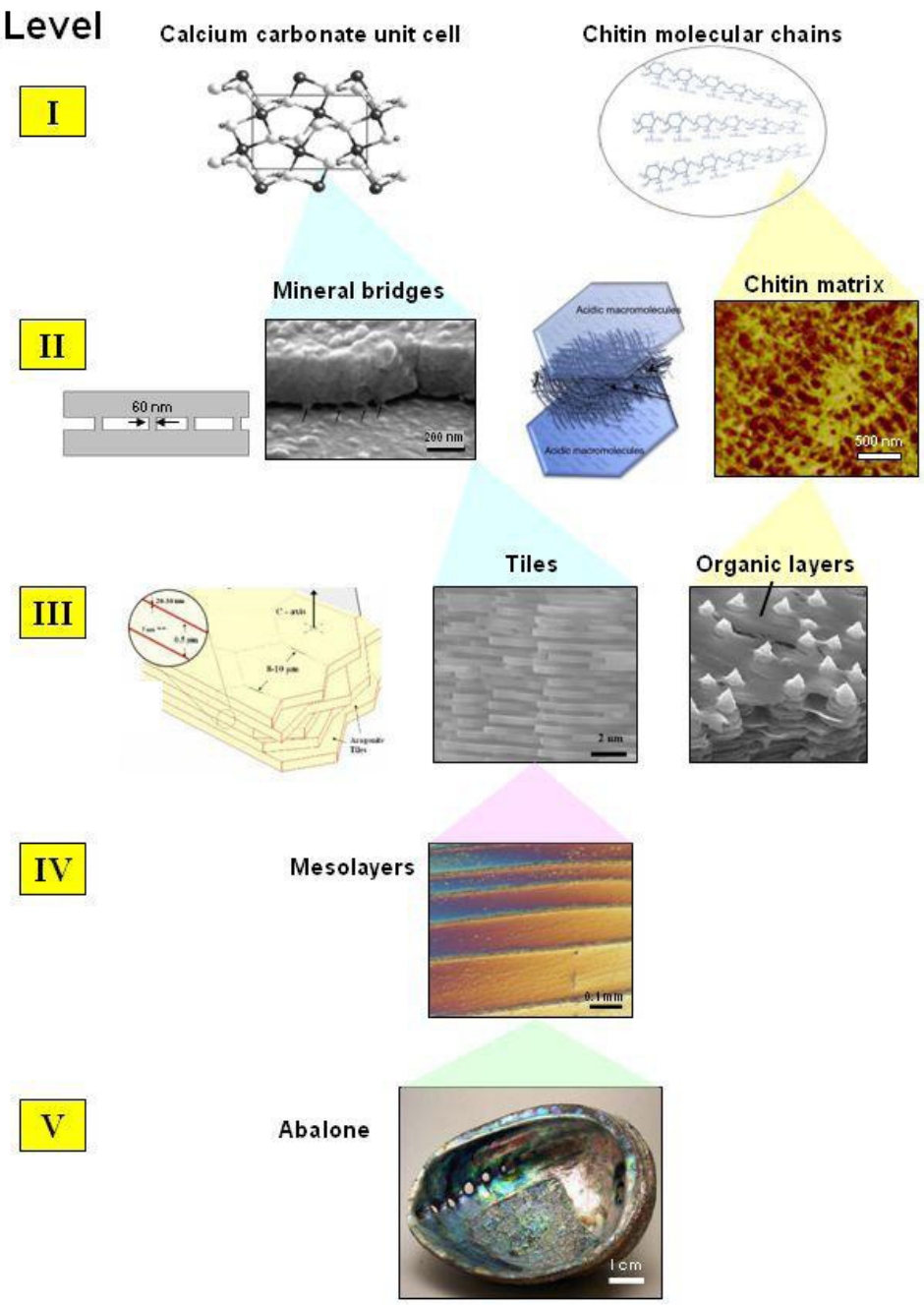

Figure 2.5: Hierarchical structure (5 levels) of the abalone nacre from nano-, micro-, to meso- to structural length scales. (*source:* Meyers et al. 2010)

2.1.2 Mechanical Behavior of Nacre: Early Work

Much work has been done on quantifying the mechanical properties of nacre. In 1977, one of the earliest experiments was reported by Currey (Currey 1977). He performed tensile, compressive, and bending tests on many bivalves, gastropods, and cephalopods. Results concluded that the bending fracture strength ranged between 56 to 116 MPa. The characteristic stress-strain curves show an elastic region followed by plastic behavior before failure. In 1988 Jackson (Jackson 1988) gave values of elastic moduli at approximately 70 GPa (dry) and 60 GPa (wet) and tensile strength of approximately 170 MPa (dry) and 130 MPa (wet) in nacre from the shell of a bivalve mollusc, *Pinctada imbricata*. In another study in 1990 Sarikaya et al. (Sarikaya 1990) reported a fracture toughness of 8±3 MPa $m^{1/2}$ of nacre in four-point tests and a fracture strength of 185±20 MPa in three-point bend tests. These results are above most conventional ceramics and comparable to ceramic matrix and metal matrix composites.

2.1.3 Compression Studies of Abalone Nacre

Quasi-static compression and tension tests were performed previously by Menig et al. (Menig et al 2000) and Lin (Lin 2008b). Lin et al. results are presented in Figure 2.6, they predict a 50 percent failure probability occurring at approximately 250 MPa for compression perpendicular to the layered structure. This is lower than previous results by Menig et al. (Menig et al 2000) of approximately 540 MPa;

however, both results are within one order of magnitude and probably due to slight differences in specimen preparation. It is important to note that because of irregularities in the shell, the results were presented with use of a statistical analysis to quantitatively evaluate the mechanical properties. Therefore the Weibull distribution (Weibull 1951) is applied to quasi-static and dynamic compression data with purpose of giving a clear picture from a scattered range of data points. Results from both tests are presented in the Figure 2.6, the diamond makers represent the study by Menig et al. (Menig et al. 2000), and the circular markers represent the study by Lin et al (Lin 2008b). The dotted lines represent the statistical Weibull curve that would correlate to these data points, a Weibull function “m” is found for each data point, 1.84 and 2.47 for the Lin (Lin 2008b) and Menig et al. (Menig et al. 2000) studies respectively.

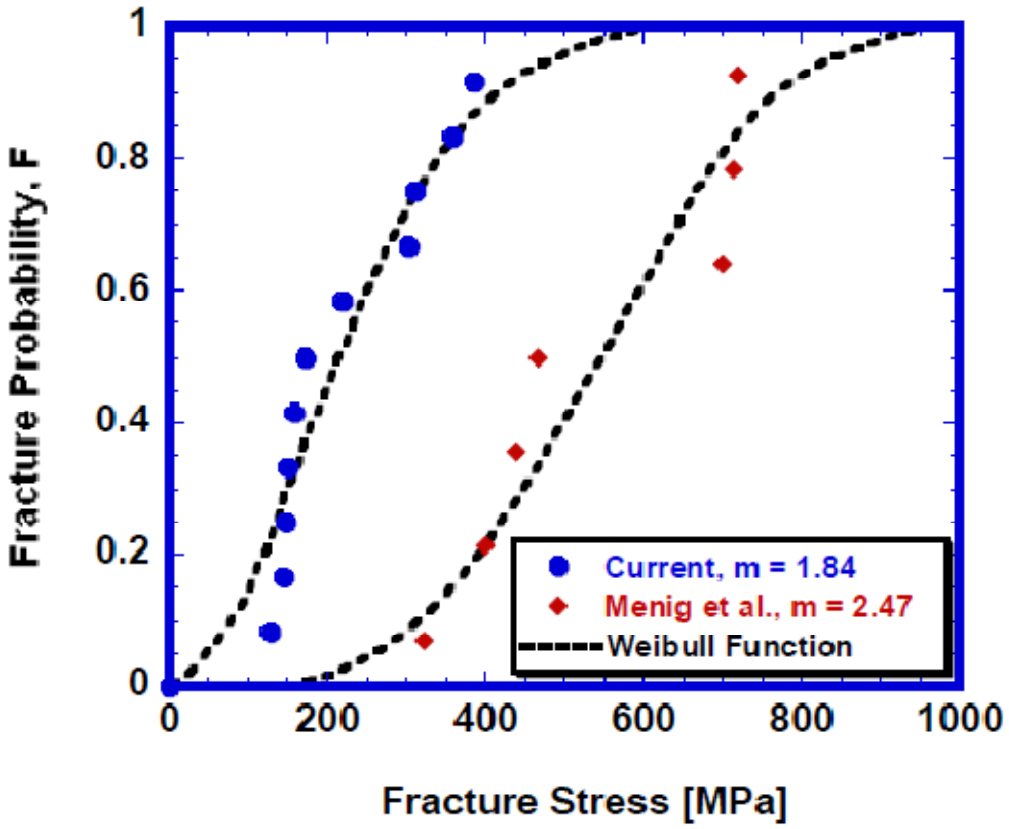

Figure 2.6: Compressive strength of freshly sectioned nacre perpendicular to layered structure (*source*: Lin 2008b).

2.1.4 Tension Studies of Abalone Nacre

Perpendicular to growth Planes

In previous work by Lin et al. (Lin 2008b) 3mm diameter pucks of nacre were removed from the shell using a diamond coring drill and mounted in cement glue then tested in tension. Thus the samples were cut so that the measurement could be done in the direction perpendicular to the planes of growth. Figure 2.7 from Lin (Lin 2008b)

shows the Weibull analysis of nacre in tension perpendicular to the layered structure. Lin found the 50% failure probability at around 5MPa, which a similar Weibull moduli in tension and compression (2-tension, 1.8-2.47-compression). It is also interesting to note that there is an extreme difference in strength in tension versus compression (ratio on the order of 100, this difference is much higher than that found in conventional brittle materials ratio on the order of 8 to 12).

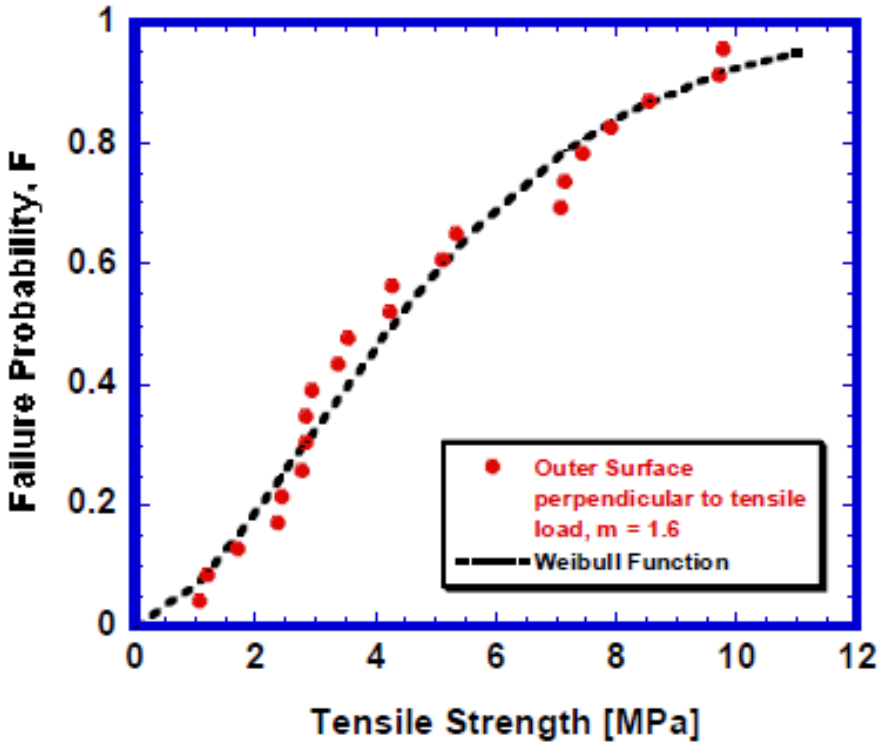

Figure 2.7: Weibull distribution of tensile strength perpendicular to layered structure (*source*: Lin 2008b).

Parallel to Growth Planes

Tensile strength studies parallel to the growth planes were additionally performed (Lin 2008b). "Dog-bone" shaped samples were sectioned from the shell and tensile tests were performed parallel to tile planes in quasi-static loading at a strain rate of 0.05 mm/min. Figure 2.8 shows the Weibull statistical analysis of the results obtained, where a 50% failure probability when a load of approximately 65 MPa was applied and the Weibull parameter was found to be 1.8. Other results from Jackson (Jackson 1988) and Barthelat (Barthelat 1977-1986) demonstrate a higher value, 170 MPa and 100 MPa respectively. It is interesting to note that in all cases the shell shows a lower tensile strength when loaded in the perpendicular direction to the tiles than in the parallel direction and shows the mechanical anisotropy of nacre. Figure 2.9 shows a summary of these results.

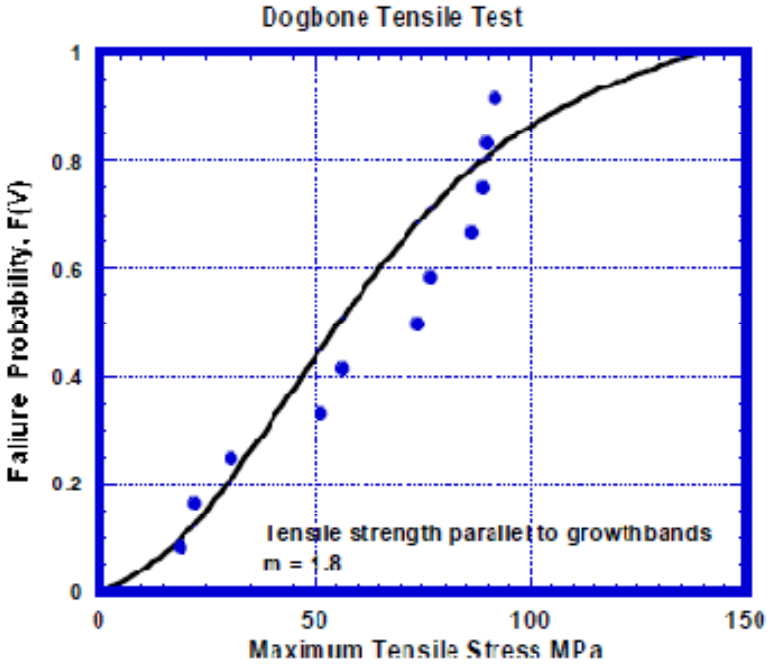

Figure 2.8: Weibull distribution of tensile loading parallel to layered structure (s*ource*: Lin 2008b).

The mechanical behavior of abalone nacre suggests three main points to be considered. Firstly, the work of fracture in monolithic calcium carbonate was approximately 3000 times less than the ones measured in nacre (Currey 1977). Secondly, previous tests show that the hydration is particularly important for the toughness of nacre, e.g. the work of fracture of dry nacre is approximately 350–450 J/m^3 and could go up to 1240 J/m^3 in wet conditions (Jackson 1988). Finally, the mechanical performance exhibited strong orientation dependence and a significant strain-rate sensitivity.

The results can be combined to show the mechanical anisotropy of nacre, recapitulated in Figure 2.9. Perpendicular to the layers, nacre exhibits great anisotropy

(3-5 MPa vs. 540 MPa). However, when the load is applied parallel to the tiles there is little difference in tensile and compressive strength (65-170 MPa vs. 235 MPa). Additionally, the shell exhibits greater compressive strength when loaded perpendicular to the tiles compared to loaded parallel to the tiles.

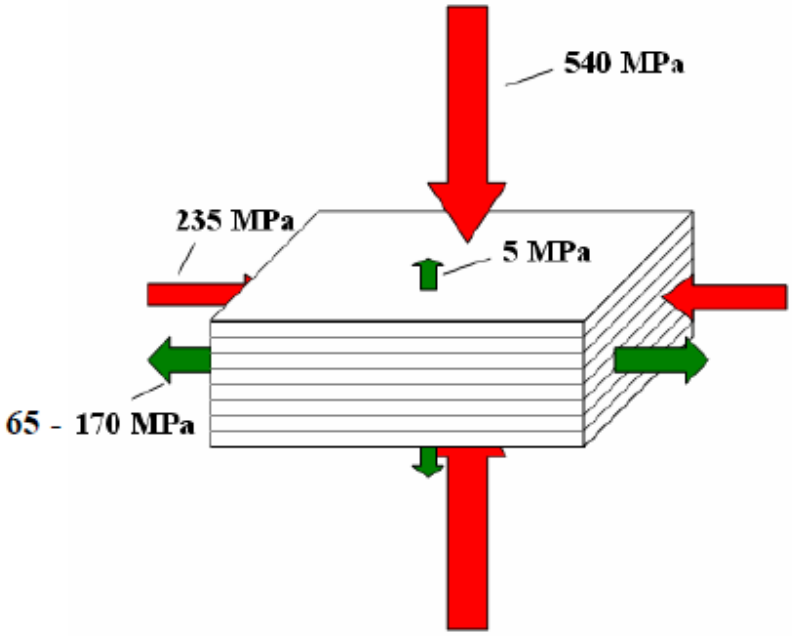

Figure 2.9: Strength of nacre with respect to loading direction, parallel lines represent growth bands (*source*: Lin 2008b).

2.1.5 Structure and Property Relationship

The high toughness exhibited by nacre has been mainly attributed to the difficult and indirect fracture path that occurs in the material. However, there are many contributions to the high toughening properties of nacre beyond that of the brick and mortar structure of nacre. The proposed toughening mechanisms are as follows:

1) Combination and organization of the tiles and the organic constituent. Sumitomo proposed (Sumitomo et al. 2008) that nacre is designed in a matter such that if a stress is applied in the normal direction to the tile plane the organic constituent will act in a ductile manner and prevent uncontrolled crack growth, this however is assuming the shell is in a hydrated state. In a dry state, the organic material acts brittle (Barthelat 2007). In addition, Smith et al. (Smith et al. 1999) suggested that the proteins making up the matrix of this organic membrane act as a strong adhesive joining the mineral tiles (Figure 2.10). Thus, when increasing the applied stress this biopolymer elongate in a step-like manner (Figure 2.11) contributing to the overall high toughness of nacre. However, previous analysis by Meyers et al. (Meyers et al. 2009) and Lin et al. thesis show that the organic layer is quite weak, and can barely support its own weight. From Figure 2.12 it can be seen that the organic membrane undergoes sagging only by carrying its own weigh suggesting the stiffness is very low. The biaxial elastic modulus of the membrane was approximated to be 100Pa Meyers et al. (Meyers et al. 2009) using classical mechanics and measuring the sagging membrane between a tile spacing of

10μm as shown by Figure 2.13. Figure 2.14 shows the calculated stress and elastic modulus of the organic layer as a function of deflection. The equilibrium diagram is shown in Figure 4.22 (b). The following parameters are defined: *a*, radius of the membrane (assumed to be circular); *w*, deflection; *p*, vertical load; *h*, thickness of the membrane; σ, radial stress on membrane. One finds that w_{max}, the maximum deflection, can be expressed in terms of known parameters:

$$w_{max} = \frac{\rho h g a^2}{4N} \tag{2.1}$$

ρ is the density; N is the tensile force per unit length which is represented by stress multiplied by unit thickness:

$$N = \sigma h \tag{2.2}$$

The biaxial stress in a membrane under its own weight is:

$$\sigma = \frac{\rho g a^2}{4 w_{max}} \tag{2.3}$$

The nominal biaxial strain is defined as:

$$\varepsilon = \frac{L-2a}{2a} \tag{2.4}$$

For the calculation of the strain, we assume θ is small. Thus:

$$sin\theta \cong tan\theta = \frac{\partial w}{\partial r} = \frac{w_{max}}{a} \tag{2.5}$$

$$L = 2\pi R \frac{\theta}{180^\circ} = 2\pi \frac{a^2}{w_{max}} \frac{\theta}{180^\circ} \tag{2.6}$$

They assumed the density of the organic layer to be 1.5 g/cm3. The thickness of the membrane is taken to be 30 nm. Two circle radii (assumed shape between sagging points of the membrane) are considered: 2.5 and 5 μm. This is consistent with tile size of approximately 5-10 μm.

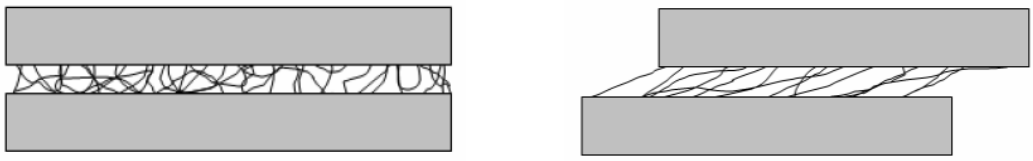

Figure 2.10: Organic layer acting as a viscoelastic glue (*source*: Lin 2008b).

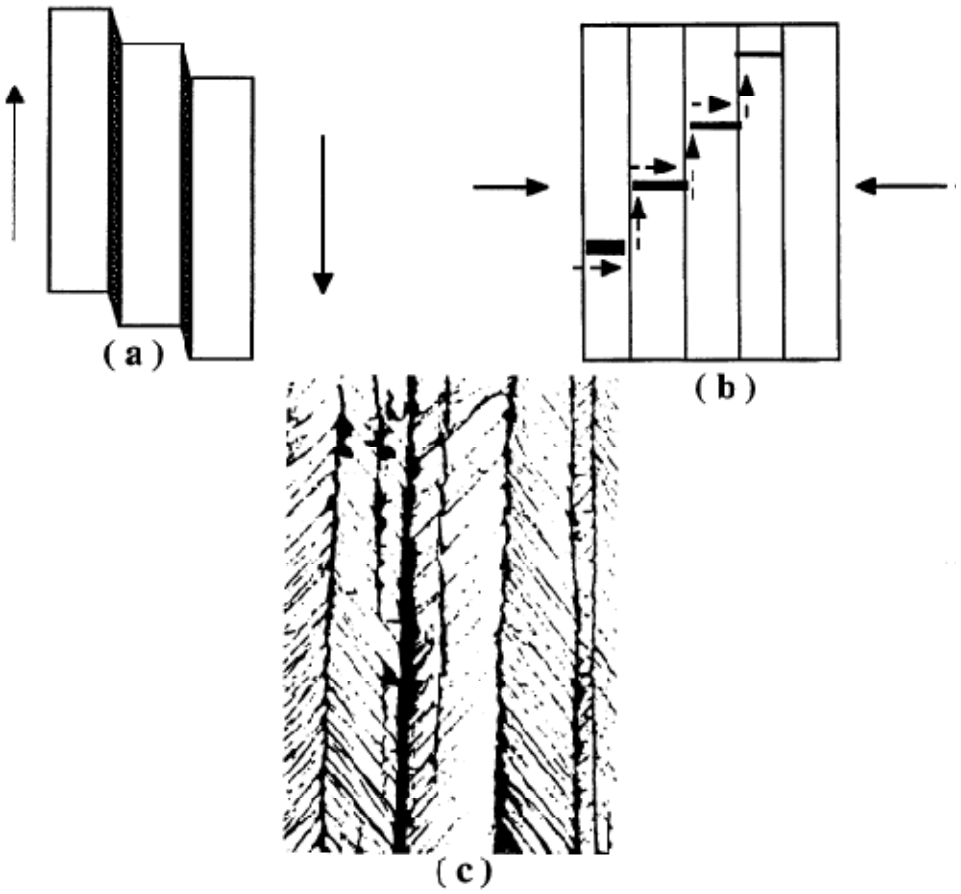

Figure 2.11: Principal mechanisms of damage accumulation in shells: (a) viscoplastic deformation of organic layers; (b) crack deflection by organic layers; (c) delocalization of damage (*source*: Menig et al. 2000).

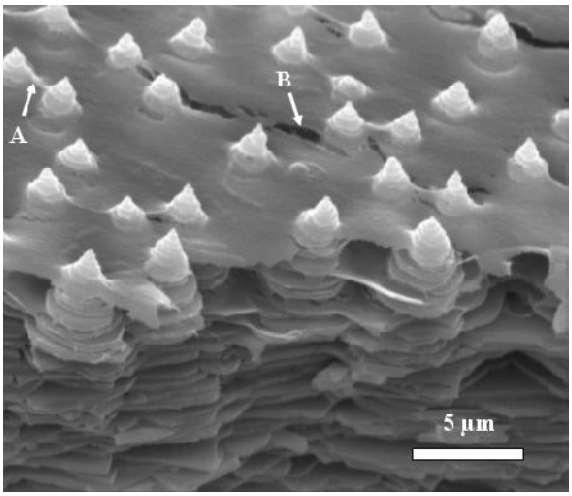

Figure 2.12: Side view of intermediate tile growth through organic layers on flat pearl five weeks after implantation (*source*: Lin 2008b).

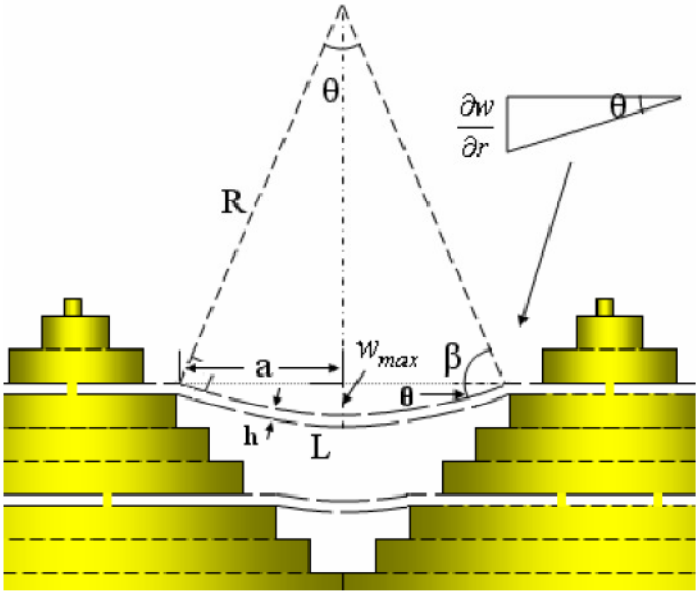

Figure 2.13: Schematic showing terraced growth and organic membrane sagging under its own weight (*source*: Lin 2008b).

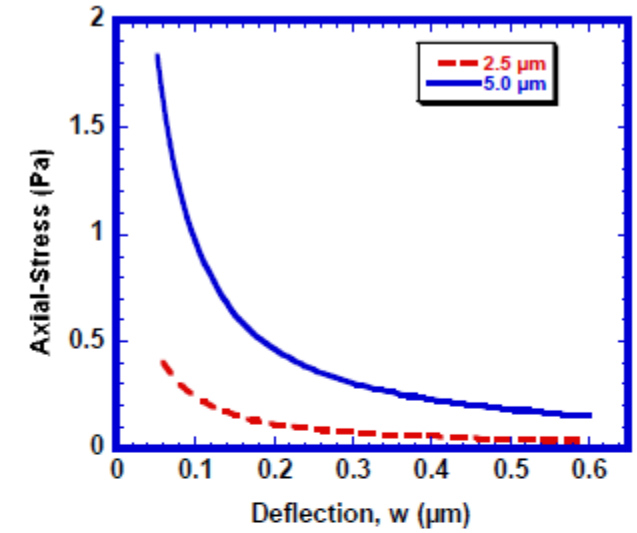

(a)

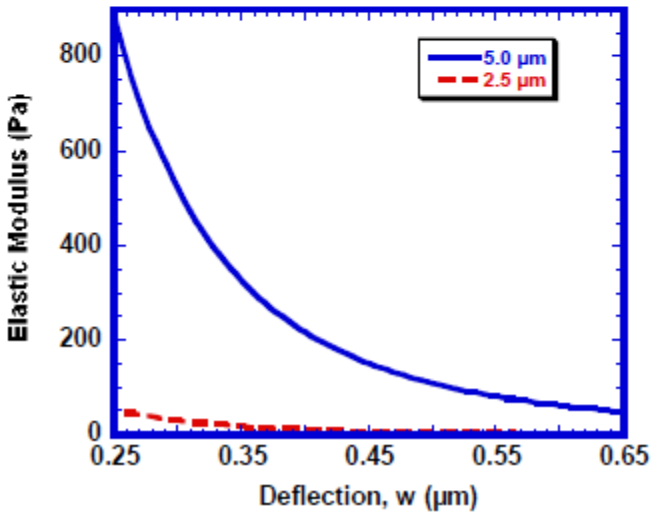

(b)

Figure 2.14: Calculated (a) stress, and (b) elastic modulus of organic layer as a function of deflection for two circle radii (assumed shape between sagging points of the membrane) are considered: 2.5 and 5 μm (*source*: Lin 2008b).

2) Asperities on the surface of the aragonite tiles (Figure 2.15 *source:* Lin 2008b) are also considered to attribute to the mechanical response of nacre. Wang et

al. (Wang et al. 2001) and Evans et al. (Evans et al. 2001) hypothesis that a stress where inelastic deformation occurs, these asperities contribute to the shear resistance between tiles.

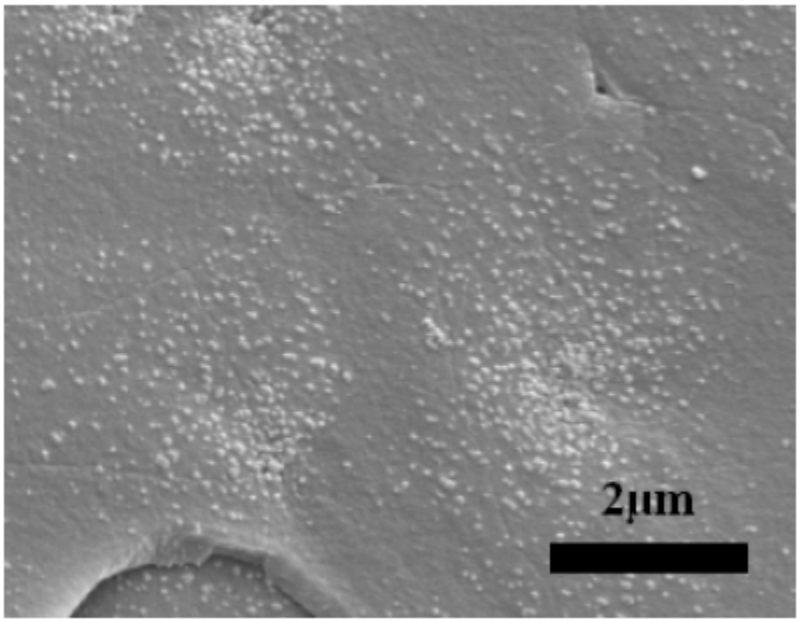

Figure 2.15: Asperities, many of which are remnants of mineral bridges, concentrated at the center of an aragonite tile after 9 hours of deproteination (*source*: Lin 2008b).

3) Mineral bridges are also considered as great providers of toughness. Song et al. (Song et al. 2003, 2004), Velazquez-Castillo et al. (Velazquez-Castillo et al. 2006) Meyers et al. (Meyers et al. 2008) confirmed the existence of interlamellar mineral bridges that are approximately 50nm in diameter. These mineral bridges are shown in different views in Figures 2.16, 2.17, and 2.18. These mineral bridges reinforce weak interfaces and are considered to be the main source of the weak tensile strength observed in the direction

perpendicular to the layered structure. Lin and Meyers predict (Lin and Meyers 2005) that because of the small diameter of the bridges, the tensile strength depends on the theoretical strength and not determined by the critical flaw size. Additionally, the distribution of the bridges of the bridges is optimized so that they act as a crack deflection mechanism.

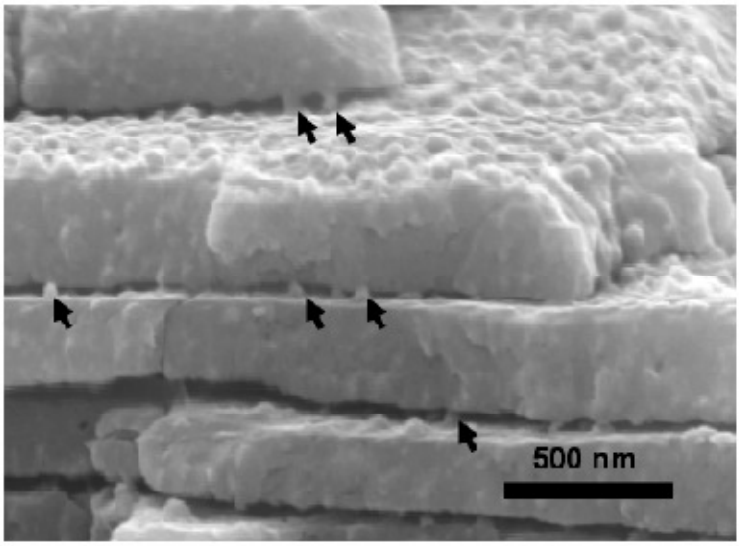

Figure 2.16: Mineral bridges (marked by arrows) between aragonite tiles after 9 hours of deproteination (*source*: Lin 2008b).

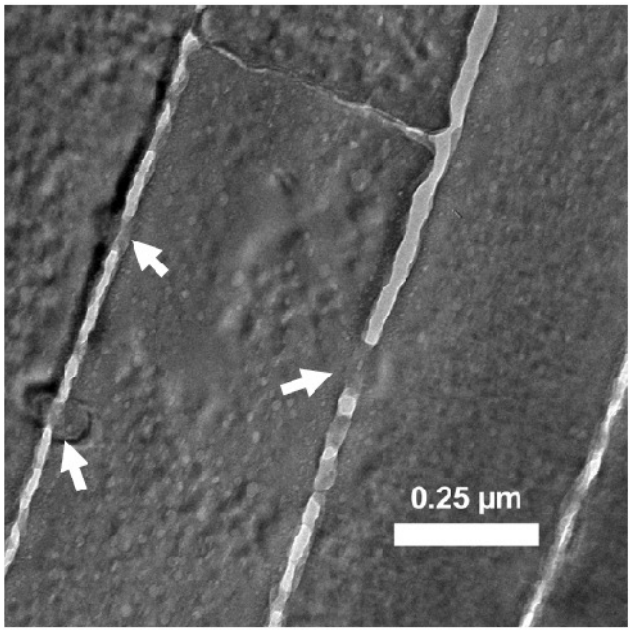

Figure 2.17: Transmission electron micrograph of nacre crossection showing mineral bridges between tile interfaces (*source*: Lin 2008b).

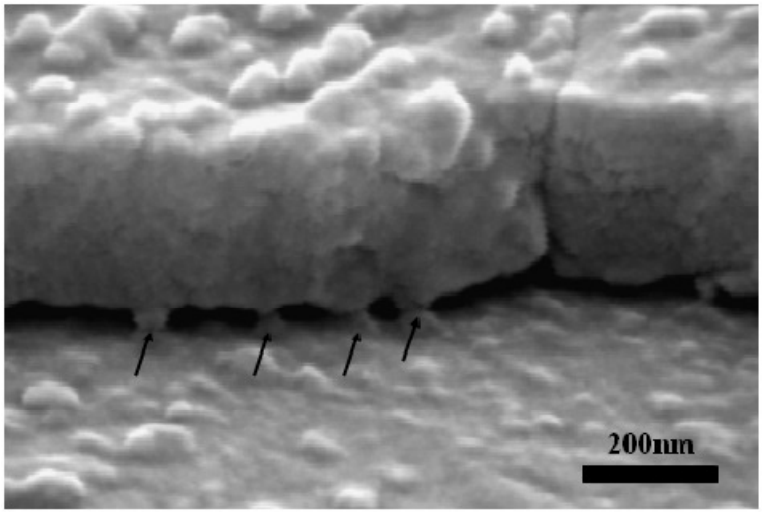

Figure 2.18: Mineral bridges (marked by arrows) between tile layers (*source*: Lin 2008b).

It is suggested the actual mechanism of toughening of abalone nacre is the combination of all three components combined synergistically. As plastic deformation takes place, the breakage of mineral bridges may form the asperities that resist shear. The organic constituent then acts as an organic glue. Figure 2.19 depicts schematically the toughening methods.

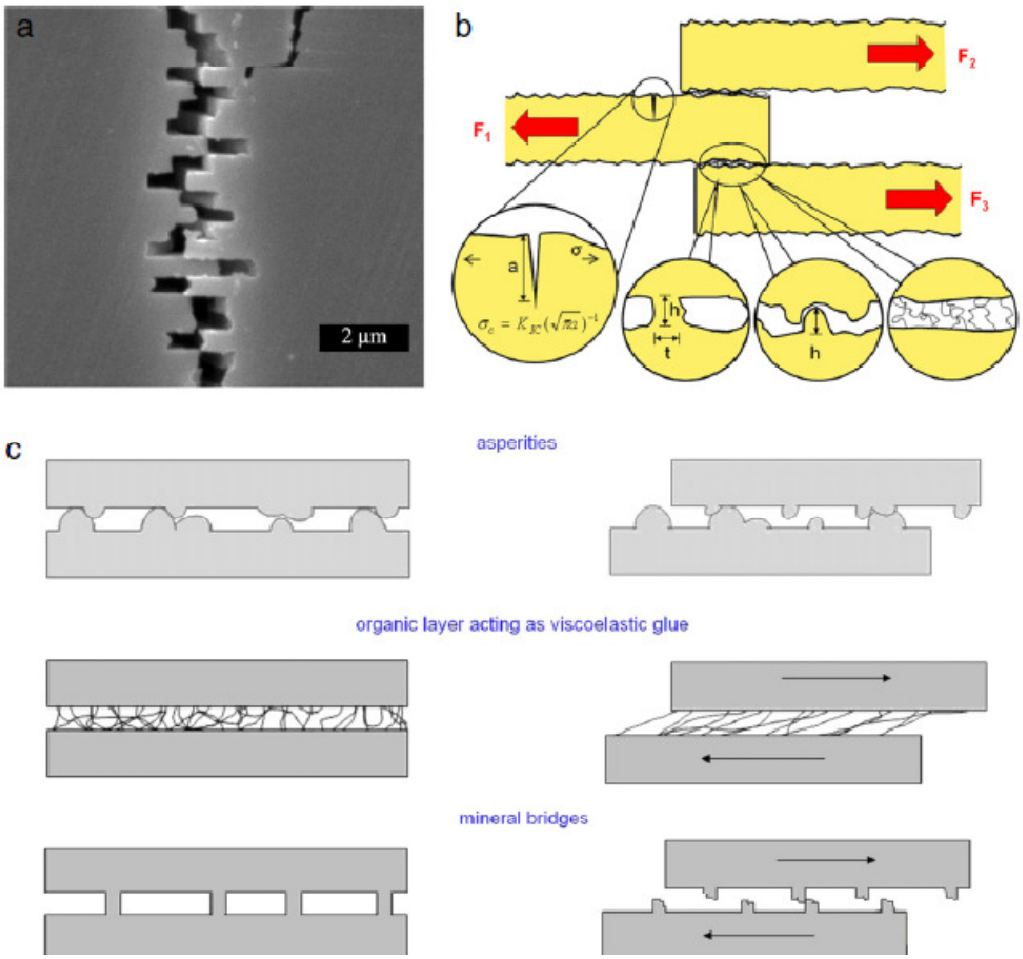

Figure 2.19: Origin of toughening in nacre: (a) SEM micrograph showing sliding of tiles in tensile loading; (b) balance between tile fracture and intertile shear; (c) details of three mechanisms of intertile shear: asperities, organic layer acting as viscoelastic glue, and fracture of mineral bridges. (*source*: Meyers et al. 2010).

However, there are other theories that have been attributed to the energy dissipation beyond the brick-and-mortar structure of nacre. These other mechanisms are:

1) The hierarchical structure of nacre ranging to the nanoscale. Gao et al. (Gao et al. 2003; Ji and Gao 2004; Gao 2006; Yao and Gao 2008) showed that in nanocomposites show a structure where the mineral particles are at a nanometer size so that strength is optimized and it allows for a high tolerance of flaws. The strength (measured by hardness) decreases as the size becomes larger. This decrease in strength occurs because the existences of flaws are in greater dimensions as the sample size is increased. The decrease in hardness is connected to the larger ease of generation of defects as the indentation size is increased. Toughness, or the ability to resist crack propagation, contrarily increases (Figure 2.20). As stated before, minerals reach the theoretical strength value when the scale is reduced to a nanometer scale. Additionally, Fratzl et al. (Fratzl et al. 2007) showed that by having a layered structure with two materials of two distinct elastic moduli can lead to a shielding/anti-shielding effect at the crack tip.

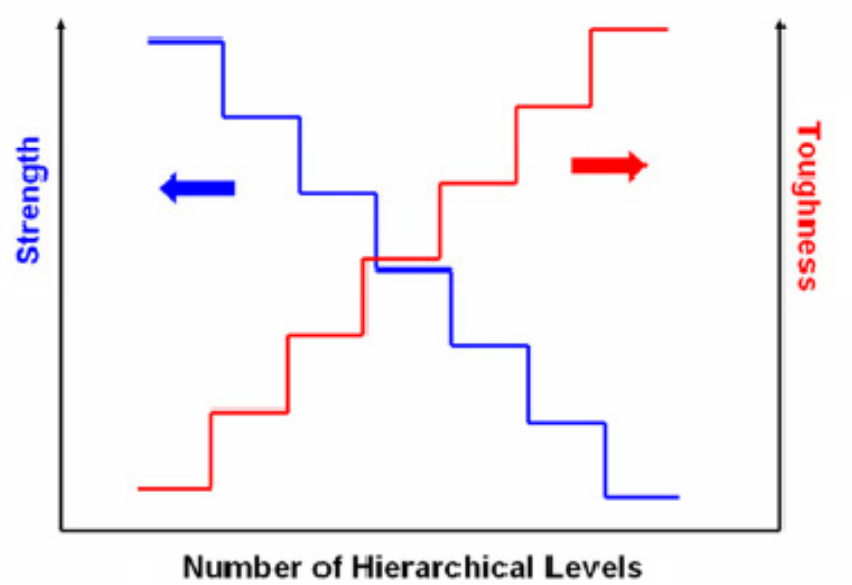

Figure 2.20: Strength and toughness as a function of number of hierarchical levels. (*source*: Meyers et al. 2010)

2) The shape and position of the aragonite tiles are also believed to be toughening mechanisms:

    a. Katti et al. reported a mismatch of layering of the aragonite tiles, e.g. the layers of tiles are not placed one over another, but 'interlocked' (Figure 2.21). This interlocking demonstrated to have an important role of the behavior by restricting a catastrophic failure of the nacre. (Katti et al. 2005; Katti & Katti 2006)

    b. Barthelat (Barthelat 2007) reports that additionally, the waved surfaces sometimes perceived in the aragonite tiles can also act as a lock and prevent tile sliding.

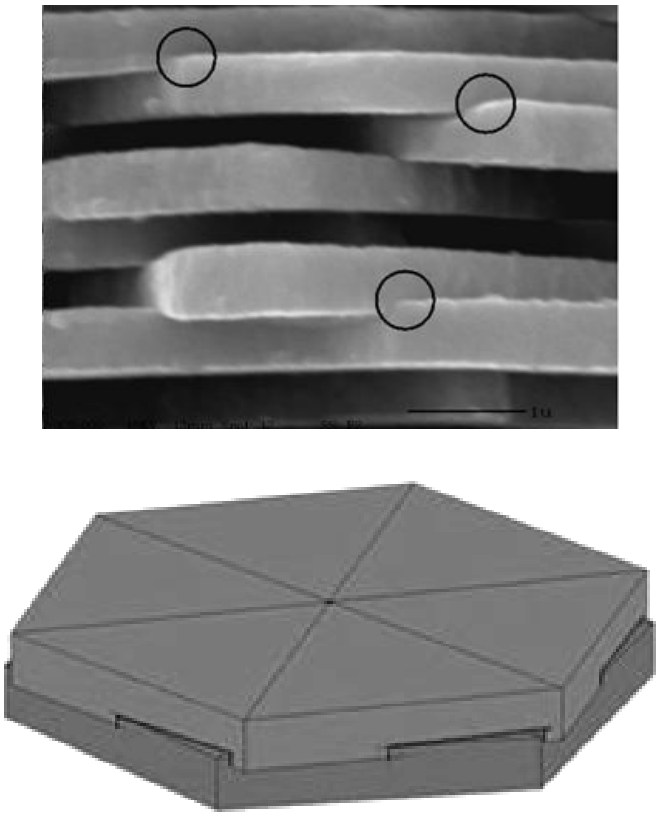

Figure 2.21: SEM micrograph showing interlocks in nacre. Schematic representing the mismatch in layering giving rise to interlocks (*source*: Katti & Katti 2006)

2.2 Growth and Biomineralization

Much effort has been done to understand the growth and formation of the abalone shell, however, for the purpose of this study the study reported by Lin and Meyers (Lin 2008a) is the most relevant. This past study investigated the various transition periods which occur during the process of shell formation.

Inorganic $CaCO_3$ goes through morphological changes between the mesolayers (Figure 2.22a). These mesolayers, or growth bands are 8 μm thick and are 300μm apart. These differences in morphology are shown in Figure 2.22b where the growth occurs from bottom to top. These five regions were identified by tiled (A); block-like aragonite (B); organic/inorganic mix (C); organic (D); and spherulitic (E). It is worth mentioning to note that prior to the arrest of growth, the characteristic tiles are replaced by a block-like structure followed by a immense deposition of the organic layer. Lin and Meyers summarized the sequence of events that occur between the formations of a mesolayers Figure 2.23.

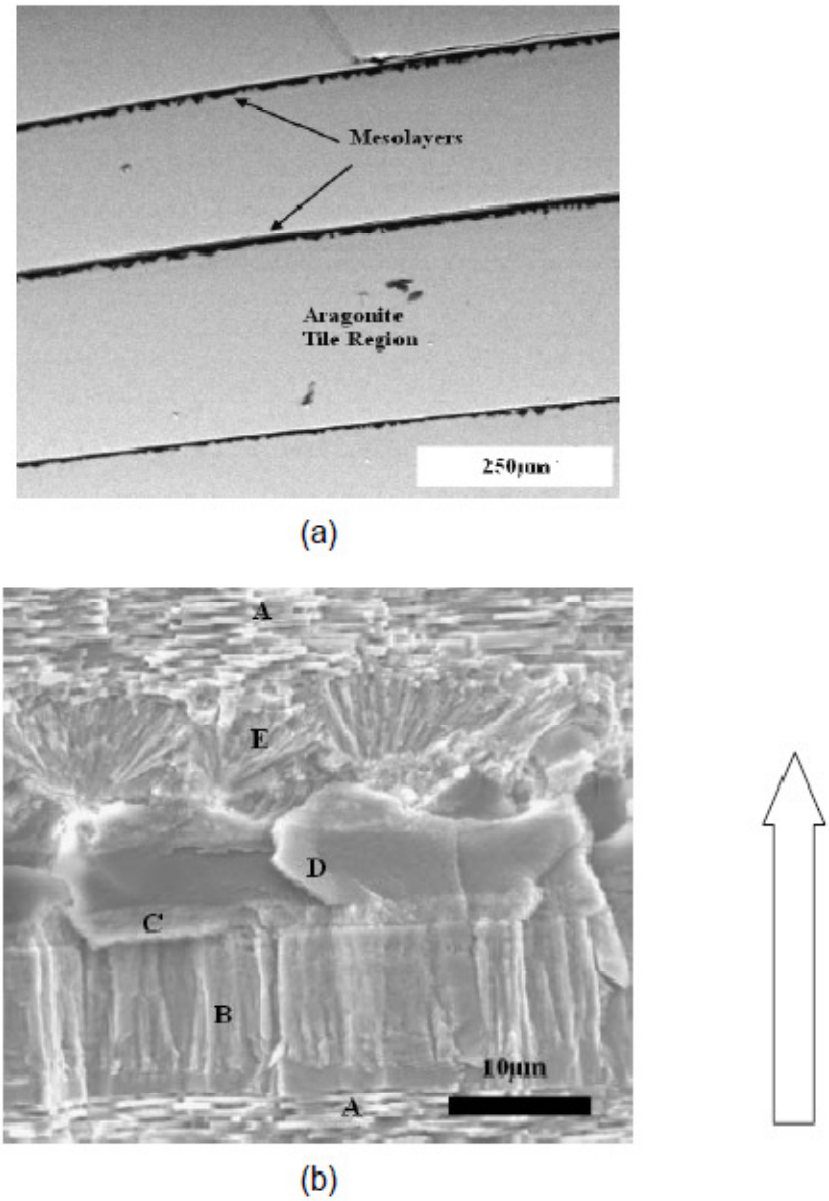

Figure 2.22: (a) Macrostructural view of a cross section of the *Haliotis rufescens* shell. Growth bands are observed separating larger regions of nacre, (b) SEM micrograph of fracture surface; direction of growth marked with arrow (*source*: Lin 2008a).

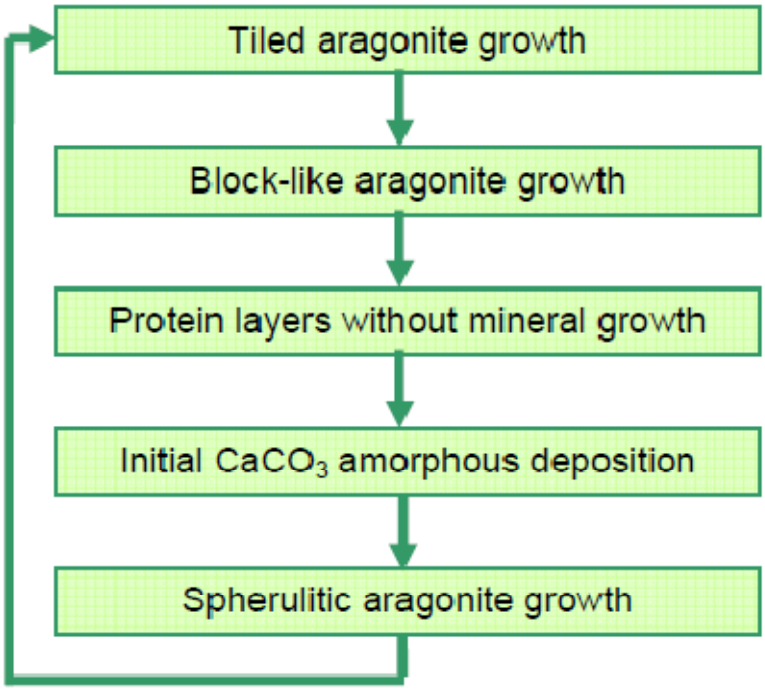

Figure 2.23 Order of events during mesolayer growth in nacre (*source*: Lin 2008a).

In the study, the flat pearl technique (as described in chapter 3) was utilized to observe the development of these different areas over a period of time. However, it is very important to note that this study was conducted with red abalone maintained in constant conditions. The abalone was maintained that is in water at ~15° C and with abalone fed regularly. The results are summarized in Figure 2.24. One week after implantation a precursor amorphous aragonite is begins to appear on the substrate. Two weeks after implantation, the precursor aragonite has spread across the entire substrate. On the lower half of Figure 2.24 it can be noticed that the morphology of deposited mineral transitions to spherulitic aragonite between the second and third week. After three weeks of implantation the tops of each spherulitic bundle appear

flattened. After four weeks of implantation, the spherulites are fully formed as a result of the divergent growth of aragonite columns along the fast growing c-axis direction. They spread apart into a lower density as growth continues after five weeks of implantation. Between five and six weeks of implantation the aragonite morphology transitions towards the regular tiled aragonite microstructure as shown at the top of Figure 2.24.

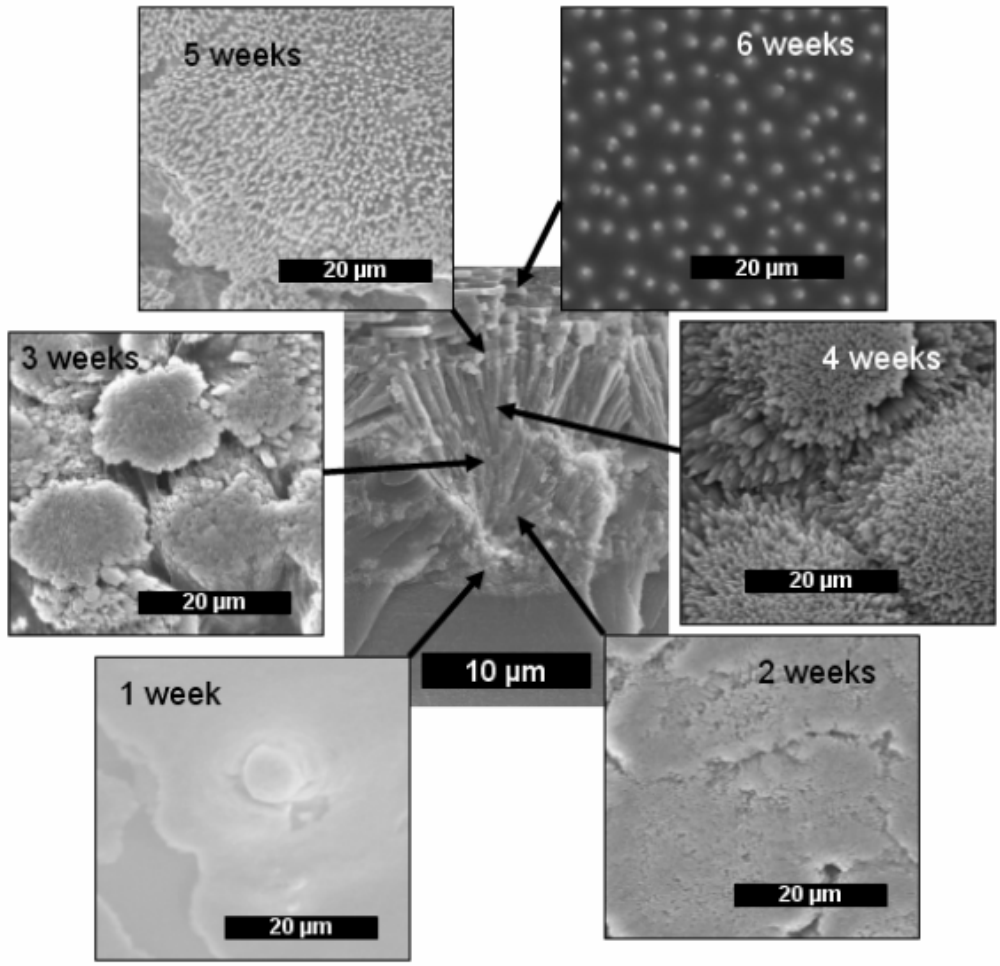

Figure 2.24: Summary of sequential growth from flat pearl and trepanning experiments (*source*: Lin 2008a).

Additionally, transmission electron microscopy was performed on the aragonite tiles. The TEM images of two samples are shown in Figure 2.25. The results show a high degree of crystallographic texture alingned normal to the plane of the tiles. The tiles show a consistency in orientation which supports the 'growth sequence through mineral bridges' theory proposed by Meyers (Meyers et al. 2009) that will be described in depth in chapter 4.

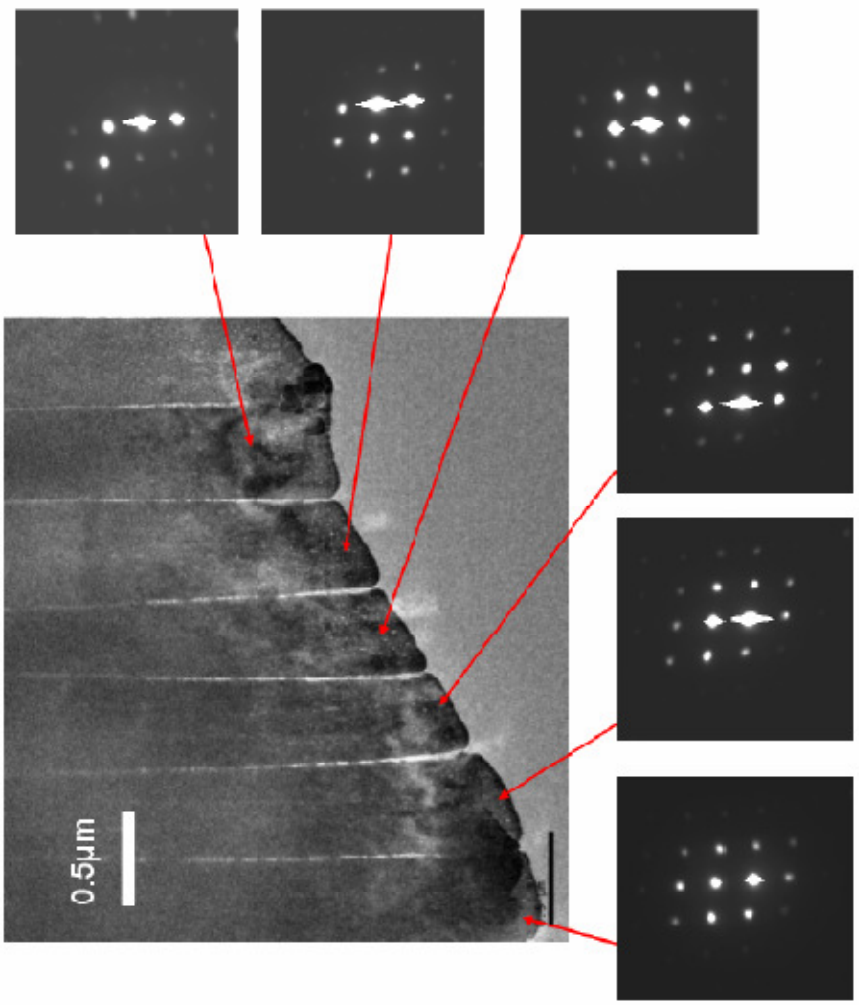

Figure 2.25: Transmission electron microscopy of tiled aragonite nacre with selected area diffraction (*source*: Lin 2008b).

Lin and Meyers (Lin and Meyers 2005) hypothesized that this transition may occur as the ends of each spherulitic needle become nucleation sites for aragonite tiles. The intermittent deposition of the organic matrix which is believed to inhibit crystal growth (Bevelander 1980) molds the spherulitic aragonite needles into an increasingly laminate structure, eventually reaching the steady-state aragonite tile formation. At six weeks the tops of the terraced cone tile columns can be seen to protrude through intermittent thin organic sheets. They are spaced approximately 3-5 µm apart,

indicating a density much less then the density of spherulitic needles. This theory can be further supported with the current results described in chapter 4 in where a deeper explanation will be given.

Lin (Lin 2008b) proposed that the animal forms the structure of the shell through a mechanical-chemical action, and by this also allows for the flattening observed in the shell. This mechanical interaction of the animal is believed to mold the design of the shell as it is built. The abalone has a strong muscle contraction between the foot and the shell, which approximates to equal and opposite force applied normal to the growth surface of the shell, shown schematically in Figure 2.26. As the animal moves along a surface it twists also twisting the epithelial layer in the mantle. This produces a sanding effect over the shell. This study is further supported by the results discussed in chapter 4.

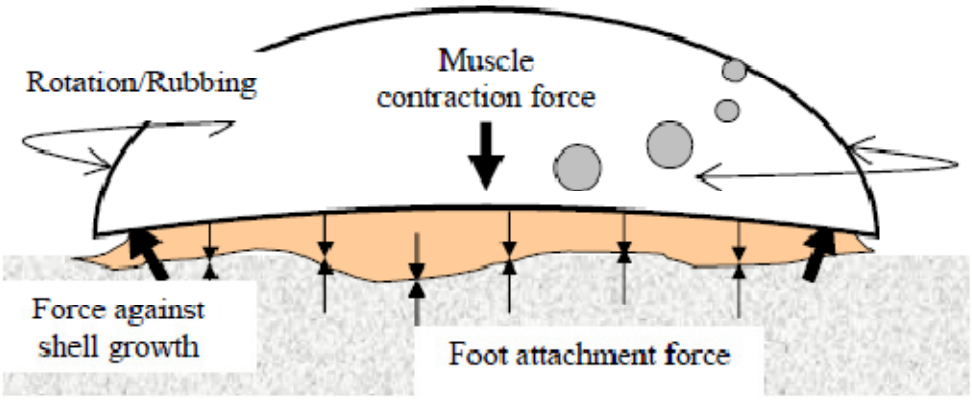

Figure 2.26: Schematic of the forces acting on the growth surface of the shell (*source*: Lin 2008b).

The growth rate was approximated to 1 tile per day, or 0.5 µm/day (5.78×10^{-12} m/s). However, as it will be demonstrated, the growth rate in abalone can vary

extremely. Lapota et al. (Lapota et al. 2000) report growth rates for red abalone to average at around 100 µm/day (in length). Zaremba et al. (Zaremba et al. 2006) reports maximum growth rates of 5µm/day, while Fritz et al. (Fritz et al. 1994) describe growth velocities averaging to 14 µm/day.

Additionally, it is noteworthy that it was reported by Lin (Lin, 2008b) that after six months of the controlled culturing of the abalone, changes in the growth patterns were noticed. Environmental changes occurred in the circulating seawater in the holding tank which caused a change from the tiled aragonite to a block-like structure identified by Su et al. (Su et al. 2002) as aragonite. This sample was reported to be brittle in comparison to previous samples. These changes were believed to be changes in the physical status of the animal due to the changes in environment. It is this issue that was of interests and was addressed and investigated in this current report.

CHAPTER 3

EXPERIMENTAL METHODS

The different experimental methods, equipment, and facilities utilized through this study will be described.

3.1 Culturing Facilities

Red abalone is held in an open water system (Figure 3.1), where sea water is directly cycled from the Pacific Ocean. The animals are fed giant kelp (*Macrocystis pyrifera*) on a regular schedule which is collected courtesy of Mr. E. Kisfaludy from the Pacific Ocean. Furthermore, abalone of adequate size and age were selected and labeled and transferred to a separate 45 liter open water fish tank so that environment could be monitored and controlled in accordance to the particular experiment. This tank had direct access to continuously circulating sea water, providing a natural environment with steady pH. Animals were continued to be fed giant kelp (*Macrocystis pyrifera*) at different schedules and the mean temperature was controlled. Three experiments were carried out, varying average temperature and feeding rate of the animal (Table 3.1).

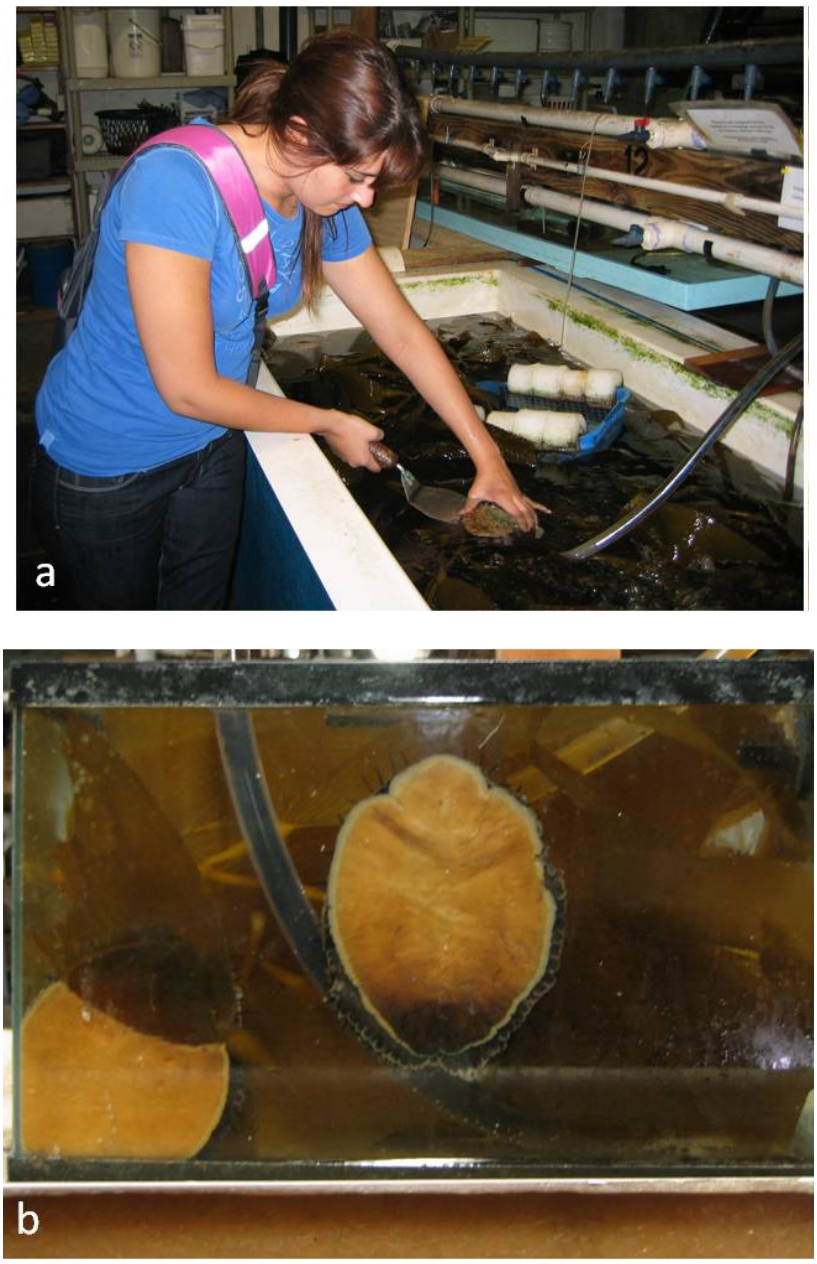

Figure 3.1: Abalone culturing facilities (a) Large open water tank and (b) 45 liter open water fish tank at the Scripps Institution of Oceanography.

Table 3.1: Experimental conditions; temperature and dietary condition.

Condition	Temperature of water	Feeding Schedule
1	~21° C	Regularly
2	~15° C	Regularly
3	~20° C	Not Fed

3.2 Specimen Collection, Preparation, and Characterization

3.2.1 Flat Pearl:

The 'flat pearl' technique, first used by Wada et al. (Wada et al. 1958, 1959) then in the US by the U.C. Santa Barbara group (Fritz et al. 1994; Schäffer 1997; Zaremba et al. 1996) and later applied by Lin et al. (Lin 2008a), was utilized to extract specimens for growth observations. Glass slides 15 mm in diameter were implanted in live abalone (glued in only one spot using Superglue®) to the growth surface of the shells. The mantle was pressed back (retracted) with a flat stainless steel scalpel with rounded edges and the slides were glued to the growing edge of the animal (Figure 3.2).Various locations along the growing edge were selected. The largest quantity of slides allowed by the size and surface of the animal was implanted on each abalone. In Figure 3.2, six slides were implanted and are shown by arrows. No copper was used in the process because of the negative reaction abalones have with the metal. Once securely adhered, the mantle relocated itself over slides over the period of approximately 24 hours. The slides were implanted for periods of 1–3 weeks and then extracted weekly for examination. At least one slide from each of the abalone was

removed weekly and prepared for scanning electron microscopy (SEM) and atomic force microscopy (AFM) characterization. Before examination each slide was washed in purified water to remove salt build up. For SEM preparation, the slides where air dried and sputter coated with gold-platinum.

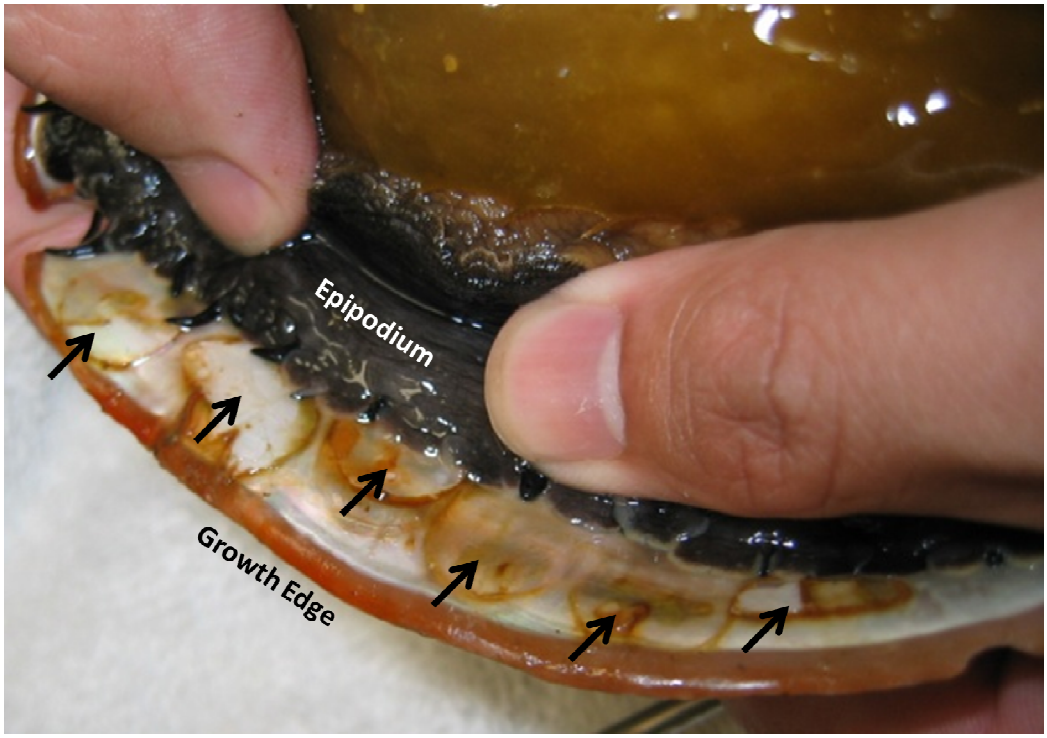

Figure 3.2: Glass slides (depicted by arrows) embedded in abalone shell**.**

3.2.2 Demineralization of Nacre:

To characterize the structure of the organic interlayer purely without interference of the major amount of mineral in the shell, the mineral has to be removed fully carefully so that the organic material is not disrupted. A common process of demineralization was employed using 0.6N HCl. Thin slices of nacre were sectioned from the growing edge of fresh abalone shells, washed in deionized water, and placed

in the diluted HCl solution at 20°C for one week. Fully demineralized samples can be seen in Figure 3.3.



Figure 3.3: Completely demineralized abalone nacre. Separation of layer occurs as the mineral is removed and the material looses most of its structural integrity.

3.2.3 Structural Characterization of Epithelium:

Tissue from the interpallial layer of mantle from the red abalone foot was removed from live specimens. Small slices (~1 cm) were cut from various sections of the abalone (Figure 3.4). Then each section was re-sectioned into two parts. Samples were CO2 critical point dried and gold-platinum coated for observation in the ESEM in high vacuum mode.



Figure 3.4: Abalone mantle pushed back revealing epithelium (depicted by arrow) prior to excision.

3.2.4 Scanning Electron Microscopy Observations on the Structure of Nacre:

A major component of this research was structural observations enabled through a Phillips XL30 environmental scanning electron microscopy (ESEM). Thus it becomes relevant to discuss some of aspects of this technique, its limiting factors, and how it was used to characterize the various specimens studied here.

The scanning electron microscope (SEM) is a very popular and useful tool utilized by materials scientists. This device allows researchers to observe and characterize easily a variety of organic and inorganic materials, including natural materials, on micrometer to nanometer scales. The scanning electron microscope was first proposed by Knoll in 1935 (Knoll 1935) and first constructed two years later by van Ardenne (van Ardenne 1938). This technique has progressed with time leading to many advances that improved the capability of SEM. Commercially; the first SEM was built by A.D.G. Stewart at Cambridge Scientific Instrument Company. This first generation model has served as the foundation for modern and modified commercial SEMs.

A basic schematic of the SEM components is shown in Figure 3.5. The microscope consists of a series of parts including a column and an electron gun to provide an electron beam that scan the specimen. The electron beam is emitted by the electron gun and then passed through electron lenses consisting of magnetic materials that are controlled by the scan coils (shown in Figure 3.5b). The electron beam scans the specimen and produces different types of electrons such as secondary electrons, backscattered electrons, and Auger electrons. Due to the distinct electronic properties

of secondary electrons, they are utilized to analyze the topography of the specimen. The backscattered electrons are also sometimes utilized because they aid in portraying differences in roughness and elemental composition. A computer system as shown in Figure 3.5a is used to obtain electron data and transform it onto an image; especially for modern SEMs this digitalized imaging system is an essential part of the model.

(a)

(b)

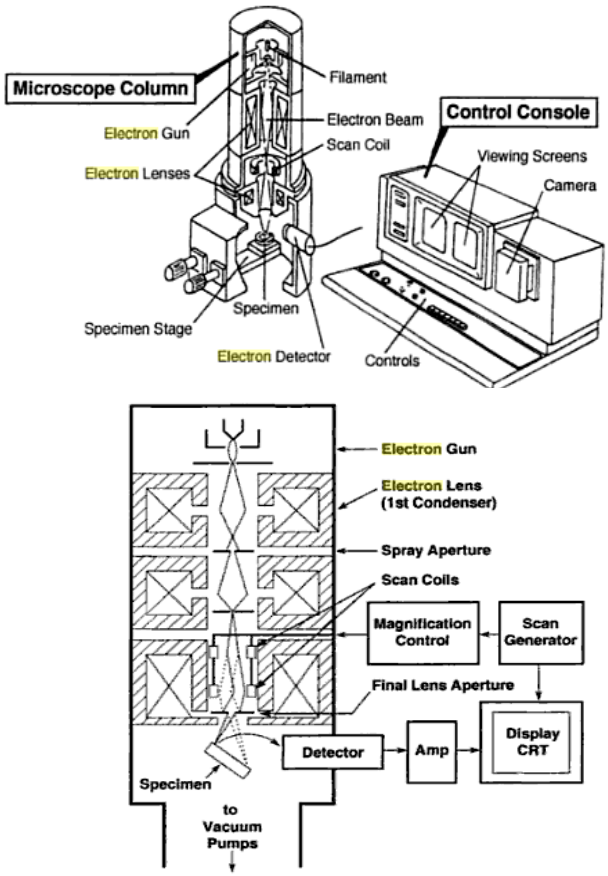

Figure 3.5: (a) Basic components and the control console of SEM, (b) the detail in the chamber of SEM (*source*: Goldestein et al. 2003).

Because SEM images are generated through the detection of electrons that are emitted from the sample that is bombarded by the highly focused electron beam, it is

important that the specimen is conductive. Because natural materials, in particular the abalone shell, are not naturally conductive it must be covered by a thin layer of gold plating. This coating layer is invisible to the SEM detector, while allowing the material to behave as conductive. In addition, localized heating may occur at the observation site, which can cause structural damage or difficult analysis process. This was mostly avoided by increasing the amount of metallization. Both an environmental SEM (FEI) at Scripps Institute of Oceanography (SIO) with accelerating voltages of 15-20 kV and a field emission SEM (FEI) with EDS at the Nano3 Laboratory in Calit2 were used for characterization.

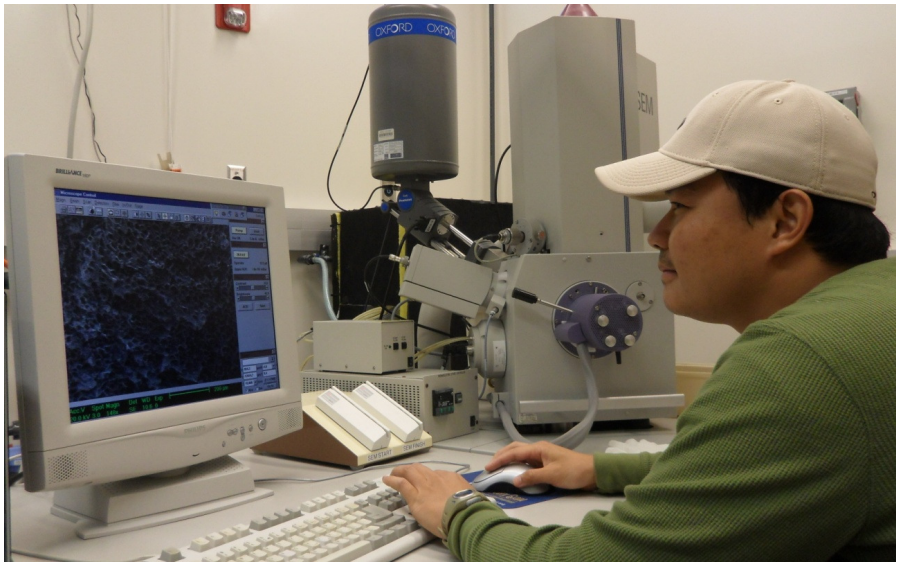

Figure 3.6: Scanning Electron Facility at Calit2 at UCSD

3.2.5 Atomic Force Microscopy:

Atomic force microscopy (AFM) was also utilized to confirm the shell formation results obtained by scanning electron microscopy. The AFM cantilever scanned the top surface of the growth specimens prepared utilizing the flat pearl method (see section 3.2.1) and positioned onto a piezoelectric mount. As the tip is brought onto proximity to the sample's surface, forces between the tip and the sample create a deflection of the cantilever in accordance to Hooke's law. The deflection is then measured by using a laser spot reflected from the top surface of the cantilever into an array of photodiodes. The AFM can be operated in various modes, most commonly static and dynamic modes. For this study, the AFM was utilized using contact mode in a static state. In other words, the cantilever remained in contact as it was dragged through the surface of the specimen.

Samples were prepared implanted growth surfaces for observations through Atomic Force Microscopy. Two instruments were used; A Veeco Scanning Probe Microscope located at the Nano3 Laboratory in Calit2, and an Atomic Force Microscope in Dr. Sungho Jin's Laboratory at the with the help of Ph.D. candidate Laura Connelly.

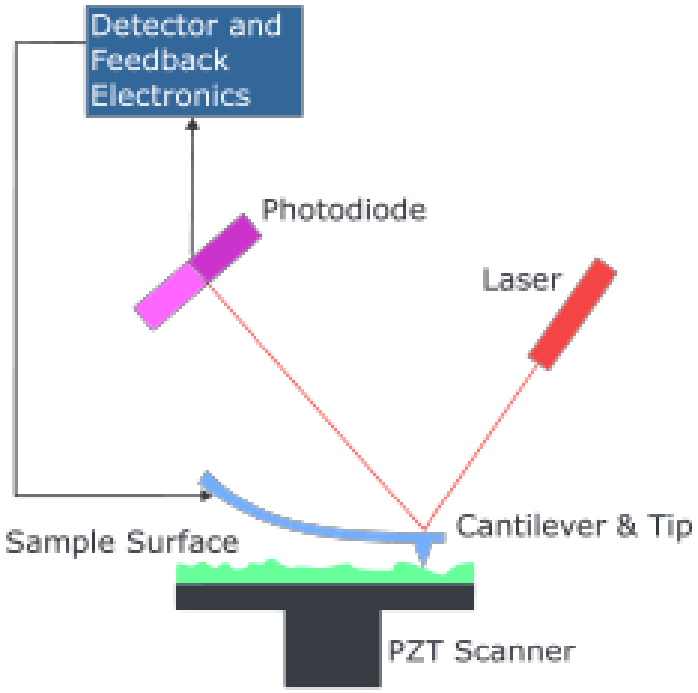

Figure 3.7: Schematic diagram of Atomic Force Microscope

3.2.6 Critical Point Drying:

Demineralized specimens of nacre sectioned from the growing edge of the abalone shell were then dehydrated completely in a progressive manner in ethanol and CO_2 critical point dried so that the structure was maintained. They were then flushed with 25%, 50%, 75%, and 100% ethanol for periods exceeding 40 minutes at each stage. They were then placed in a critical point drying machine and drenched in liquid CO_2 under high pressure. The temperature of the critical point chamber was then raised to the point in which liquid CO_2 directly becomes vapor, which freezes the material leaving the organic interlayer intact without deformation.

CHAPTER 4

RESULTS AND DISCUSSION

The following chapter has been sectioned into three main components: characterization of growth surfaces, epithelium observations, and demineralized shell and organic layer. An analysis and discussion of the results is presented within each subsection.

4.1 Characterization of Growth Surfaces

This section will describe the results of the mineral deposition on the glass slides obtained by utilization of the flat pearl method. It will become clear that the morphology of the deposited mineral varies greatly with changes in environmental conditions. This section will attempt to explain why these structural differences occur.

Flat pearl deposition experiments were utilized to expand knowledge of results obtained by Lin et al. (Lin et al. 2008a). Growth experiments were performed for a period of three weeks, following the similar methodologies utilized by Lin et al. (for detailed explanation see chapter 3). Because the tests were performed under some critical conditions, e.g. lack of nutrition, it was not possible to extend the growth period for an extreme length of period of time without the fatality of the animal which would in turn alter the results. Therefore, for comparison purposes only results taken for a period of up to three weeks will discussed here.

Tests were conducted in the three different environmental conditions demonstrated dissimilar results. The investigation in warm water (21 °C) revealed

that the aragonite tiles formed after only one week (Figure 4.1). Furthermore, the folding organic layers which are approximately 300 nm thick (marked by arrows) can be observed. Conversely, in cold water (15°C) (Figure 4.1b) or with food limitation (20°C) (Figure 4.1c), observations after one week showed only the slight start of the precursor aragonite spread across the substrate and some of the deposited mineral transitioning to spherulitic aragonite. Slides from the additional abalone were also observed and confirmed the same results. In addition, it is interesting to note, that not only was there an immense difference in the morphology of the sample, but also the amount of deposition. Figure 4.2 shows the most noticeable difference in quantity of deposition, where the coverage exhibited under a well fed and warm environment (Figure 4.2a) can be compared with conditions deficient in nutrients.

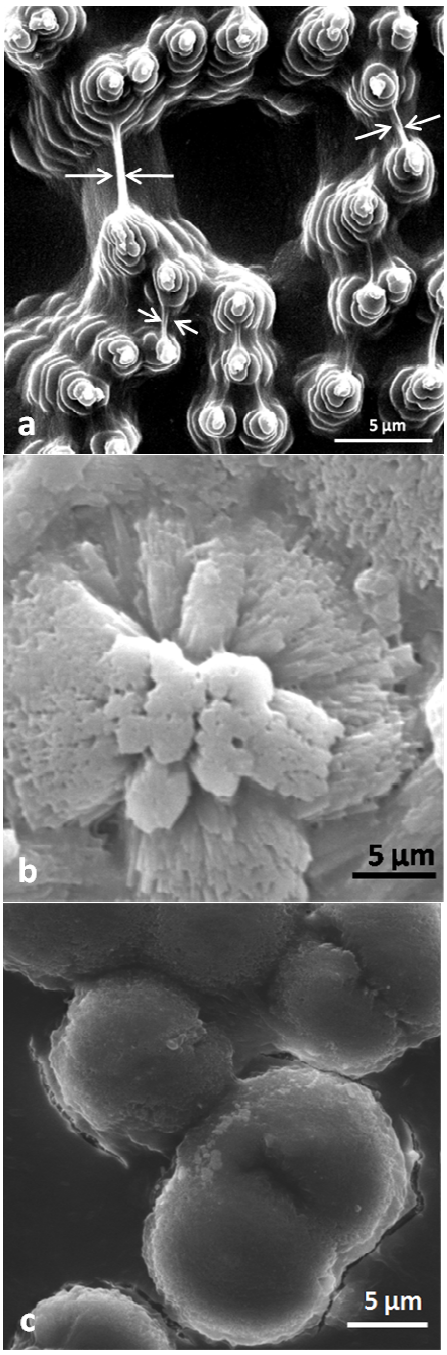

Figure 4.1: Sequential growth results 1 week after implantation. a) Growth at 21°C with abalone regularly fed; b) Growth at 15°C with abalone regularly fed; c) Growth at 20°C without food available.

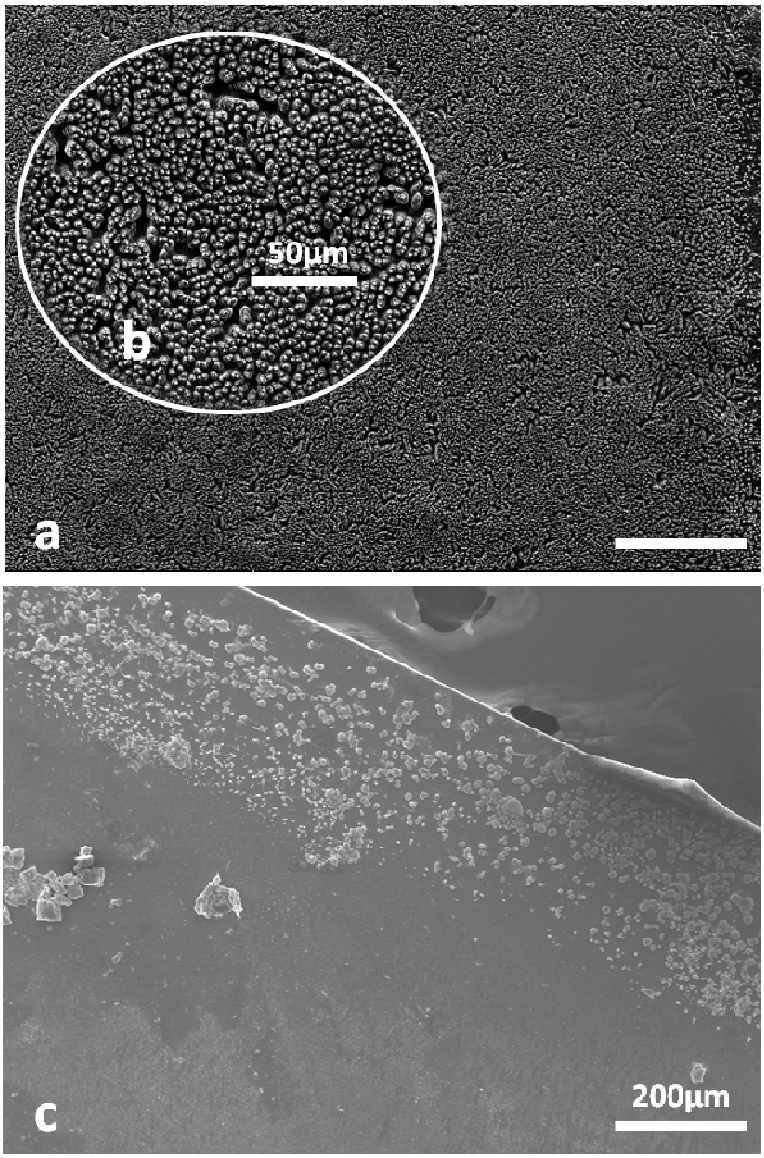

Figure 4.2: Sequential growth results 1 week after implantation. a) Growth at 21°C with abalone regularly fed showing the coverage exhibited by the tiles (top view); b) higher resolution of top view of growth at 21°C with abalone regularly fed (top view); c) Growth at 20°C without food available.

Moreover, after week 2 demonstrated similar aragonite tiles (Figure 4.3a) when the growth was conducted in warm water (21°C). In contrast, uniform spherulitic aragonite was observed in cold water (15°C) (Figure 4.3b) or under no feeding conditions (20°C) (Figure 4.3c). Interestingly, the spherulitic aragonite observed when the animal was not fed tends to be less radiated compared to the structure in colder water.

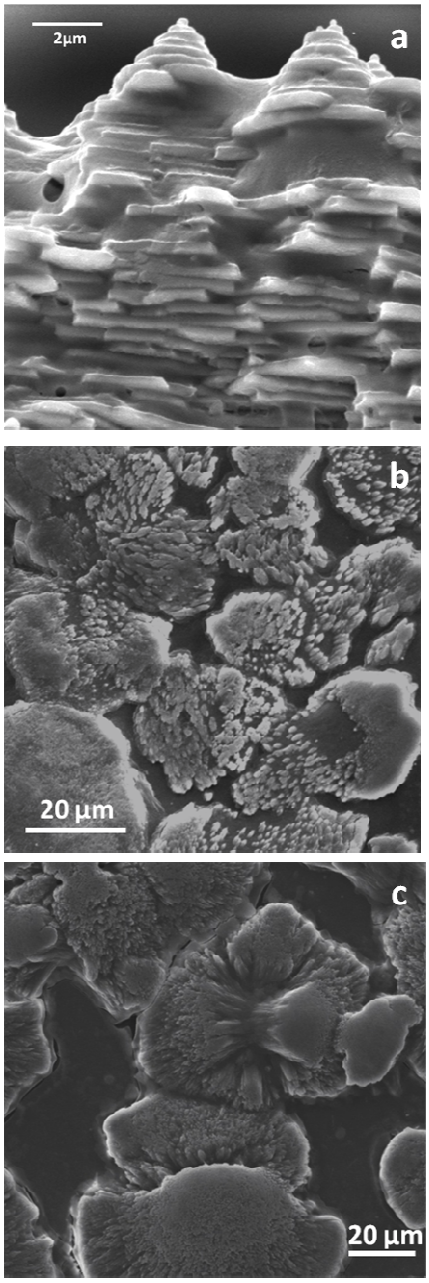

Figure 4.3: Sequential growth results 2 weeks after implantation. a) Cross-sectional view of growth at 21°C with abalone regularly fed; b) Growth at 15°C with abalone regularly fed; c) Growth at 20°C without feeding.

After three weeks of growth in warm water (21°C), a uniform and high number of staked aragonite tiles (terraced cones) were observed (Figures 4.4a and 4.4b). It can be noted from Figure 4.4a that because the height of the terraced cones is the same, an even deposition is formed. In addition, from this cross-sectional view, a continuous membrane formed by the organic layer can be observed. From Figure 5b it can be noted that the top of the terraced cones appears to be of a consistent diameter (~400 nm). On the contrary, after three weeks of implantation, the tops of each spherulitic bundle form a plateau for test at 15°C (Figure 4.4c) and test without feeding (20°C) (Figure 4.4d). In addition, the thin organic membrane can be observed (Figure 4.4c).

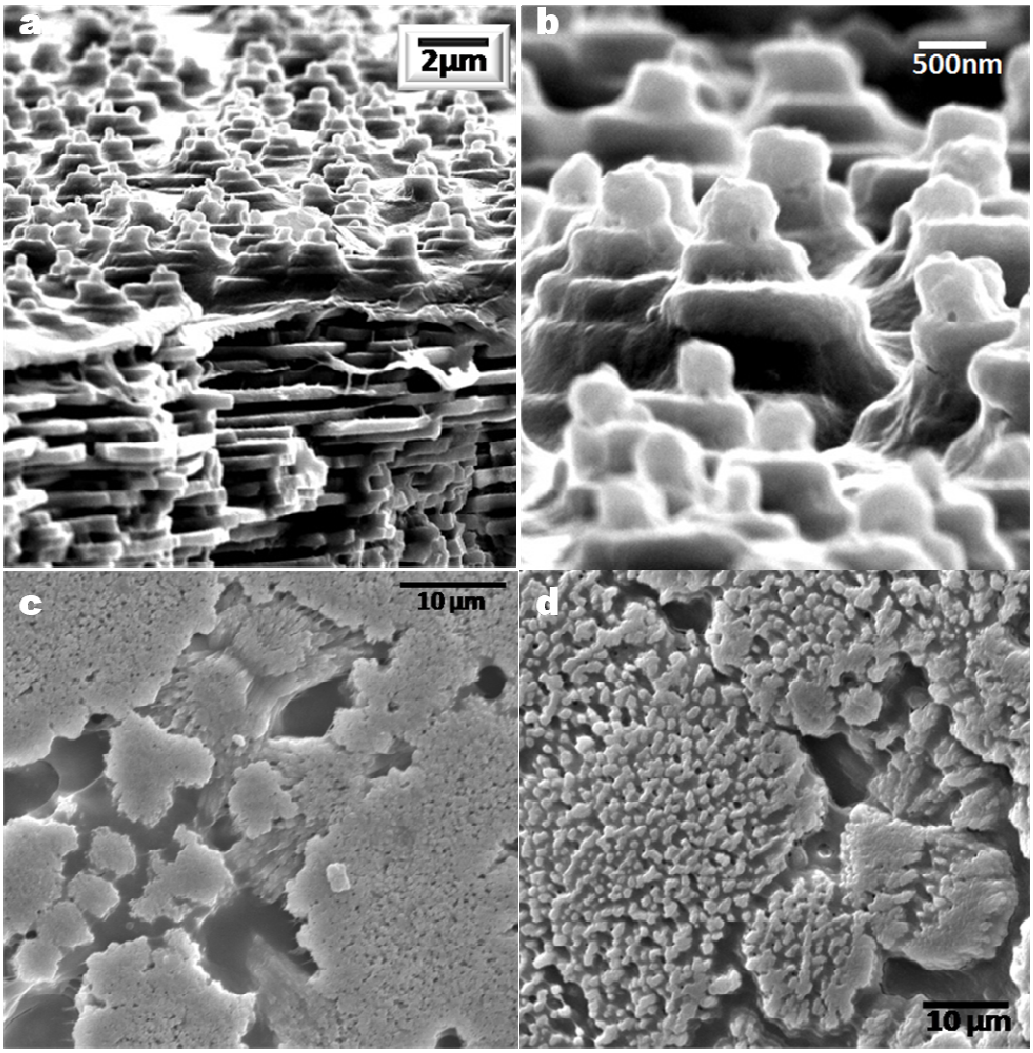

Figure 4.4: Sequential growth results after 3 weeks of implantation. a) Growth at 21°C with abalone regularly fed (cross-section); b) Detailed view of aragonite tile morphology; c) Growth in 15°C with abalone regularly fed; d) Growth in 20°C without food available.

AFM confirmed all the features observed by SEM. Figure 6 shows the growth surface in 21°C. These mineral projections (terraced cones) are approximately 2 μm high, containing about four layers from the top of the cones. This corresponds to the thickness of the tiles, (~0.5 μm). One can also see in Figure 3.5, on the sides of the protrusion, which represent terraced cones, the organic interlayer in a tent-like formation. This is similar to the configurations seen in Figures 4.2, 4.3 and 4.4, in which a thin organic layer covers terraced cones and demonstrates that the organic layer, in its fully hydrated condition, stretches under its own weight. On the other hand, it acquires substantial strength when it is dry (Meyers et al. 2009). In contrast to this, Figure 4.6 demonstrates that only the spherulite morphology is attained with growth in water at 15°C. Some distortion exists as the AFM tip does not capture very well the lateral details. It should be clarified that the rate of the transition from initial randomly arranged $CaCO_3$, a spherulitic transient phase, to final aragonite tile growth reported here is not the growth rate of the nacre, which is also affected by temperature and food availability (Steinarsson 2003). Sequential growth results discussed by Lin et al. (Lin et al. 2008a) demonstrated the shell growth required various transitory phases to reach the steady-state growth of aragonite tiles. Aragonite tiles formation was achieved after approximately 6 weeks of precursor transitory phases (this previous study was performed at 15°C and the animal was fed regularly). The growth surfaces (Figure 4.1b and 4.3b) show dominating spherulitic pattern and columnar growth which is comparable to the results for three to four weeks described by Lin et al. (Lin et al. 2008a). In contrast, when the temperature was warmer (21°C), the transitions occurred faster. At this temperature, the transitory phases cannot be observed as the

steady-state growth of aragonite tiles is reached by week one. Additionally, when the animal was not fed, the transitions occurred later. The columns observed in the limited food conditions at 20°C tend to be less radiated and the surface less smooth when compared with the growth surfaces attained at 15°C. It is believed that the predominant columnar growth of the aragonite mineral is interrupted by the deposition of thin organic intertile layer (Meyers et al. 2009). The lack of nutrients and lower temperature may reduce the production of the organic layer (chitin and proteins), which leads to an unimpeded rapid columnar growth instead of the steady-state growth of the aragonite tiles.

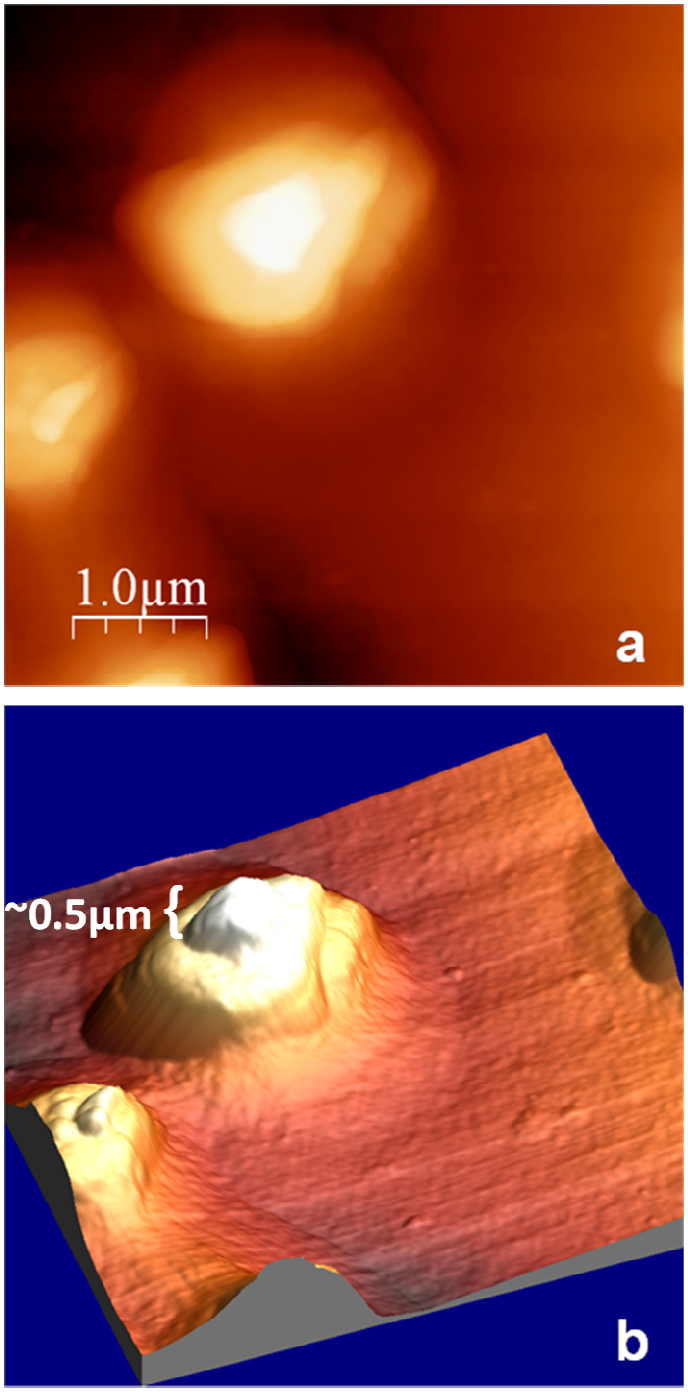

Figure 4.5: Atomic force microscopy of growth surface in 21°C showing the aragonite tile growth. a) Top view; b) Tridimensional view.

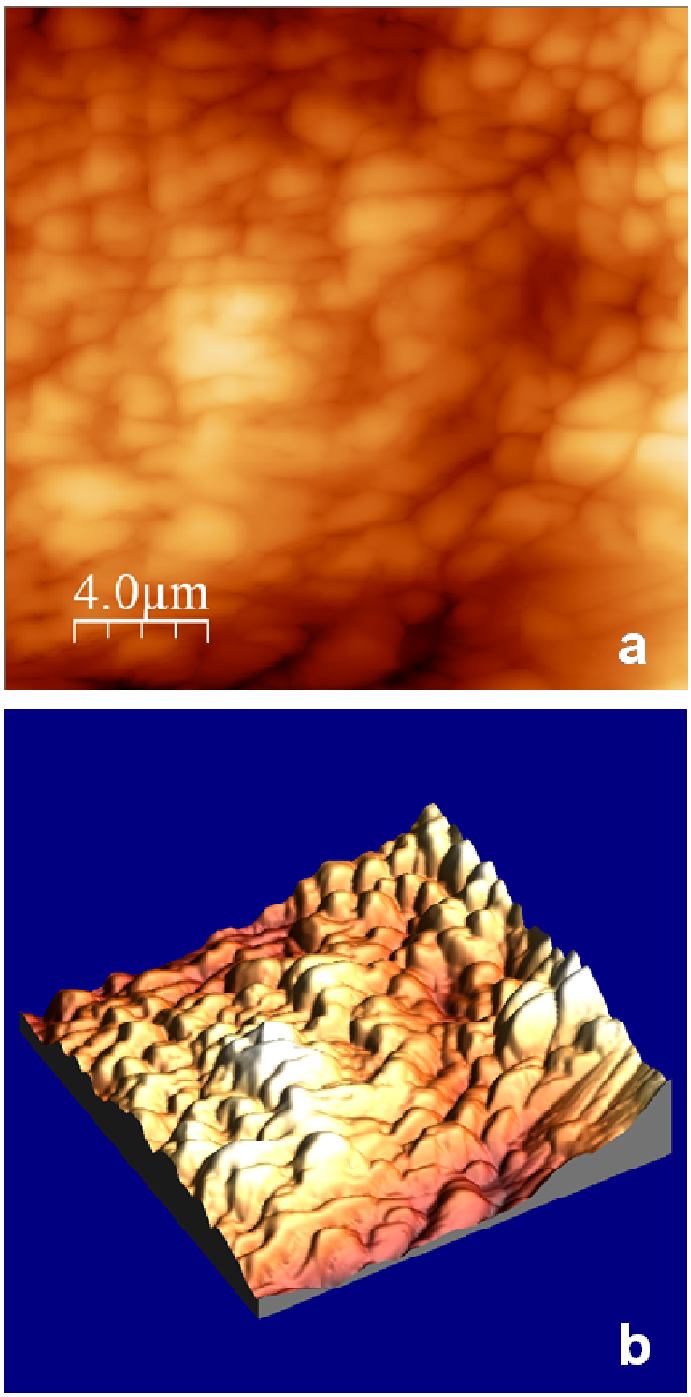

Figure 4.6: Atomic force microscopy of growth surface in 15°C showing the columnar structure. a) Top view; b) Tridimensional view.

4.2 Epithelium Observations

Inspection of the mantle reveals the secretory epithelium which is in direct contact with the inner surface of the shell (Figure 4.7). This part of the animal is the critical component in the mineralization of the shell, since it is only separated from the growing surfaces by the small extrapallial space. SEM inspection (Figure 4.7a) shows a top section of the outer surface of the epithelium (labeled I) and an area where the top surface is scraped off (labeled II). The relatively smooth outer surface of the epithelium (Figure 4.7b) suggests that the epithelium mechanically flattens the growing surface by sliding over the shell, producing a molding effect (Lin et al. 2008a) analogous to a potter molding clay. From the scraped surface one can observe that an array of channels exists inside the epithelium (detailed view of the channels shown in Figure 4.7c). Some of these channels show fibrils (Figure 4.7d). Lin et al. (Lin et al. 2008a) and Meyers et al. (Meyers et al. 2009) proposed that ions are allowed to diffuse through these channels. In addition, these channels may provide support for the synthesis of chitin and its intermittent extrusion onto the growth front (Figure 4.8).

Additionally, the epithelium consists of epithelium cells that hold microvilli which were firstly identified by Nakahara (Nakahara 1991). The microvilli have dimensions of 100 nm diameter and 400 nm height (Figure 4.9), which correlate well with the pattern of holes in the organic layer and the thickness of the tiles. Thus, it is proposed that a mechanism of templating is taking place as shown in Figure 4.10.

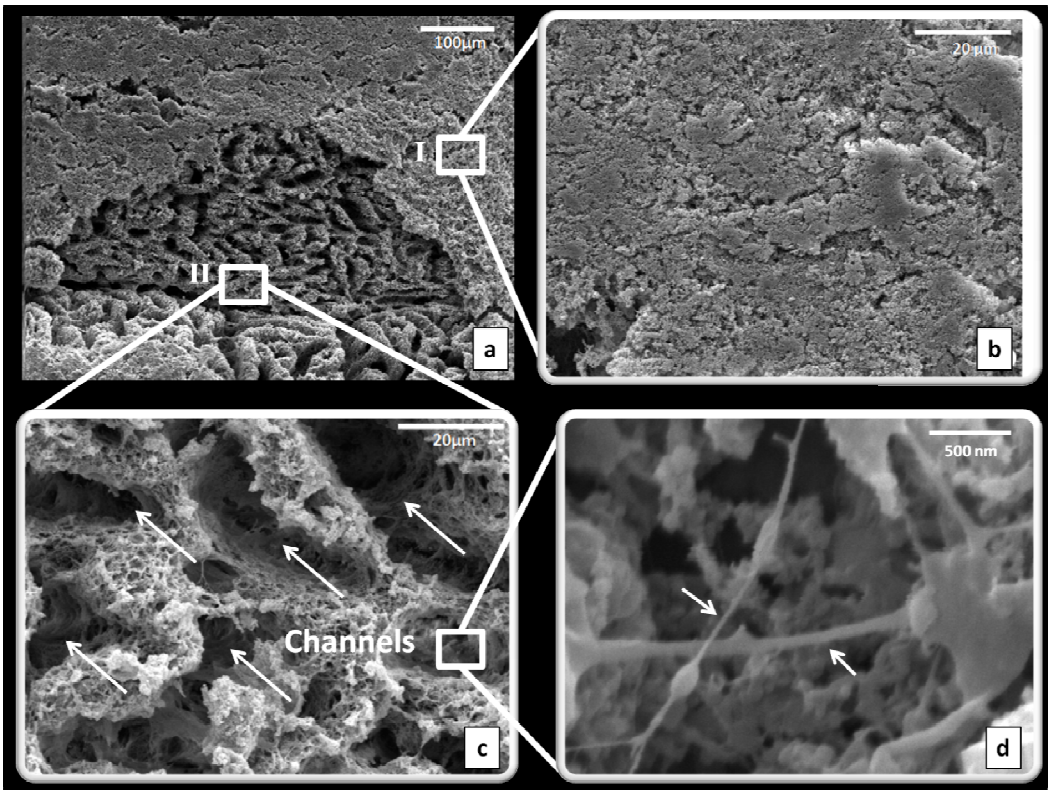

Figure 4.7: a) Sectioned epithelium; surface in contact with growing edge of shell depicting flat outer surface (I) and area where surface was scraped off (II); b) Detailed view of flat outer surface of epithelium. c) Array of channels within epithelium (channels depicted by arrows); d) Fibrils within channels (marked with arrows).

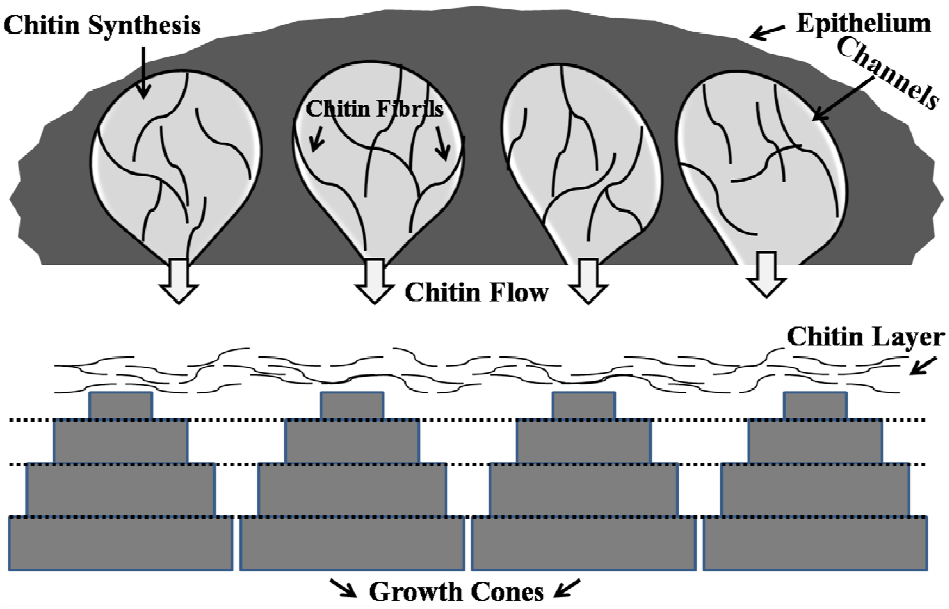

Figure 4.8: Schematic depicting hypothetical mechanism by which epithelium generates chitin fibrils and 'squeezes' them onto growth surface.

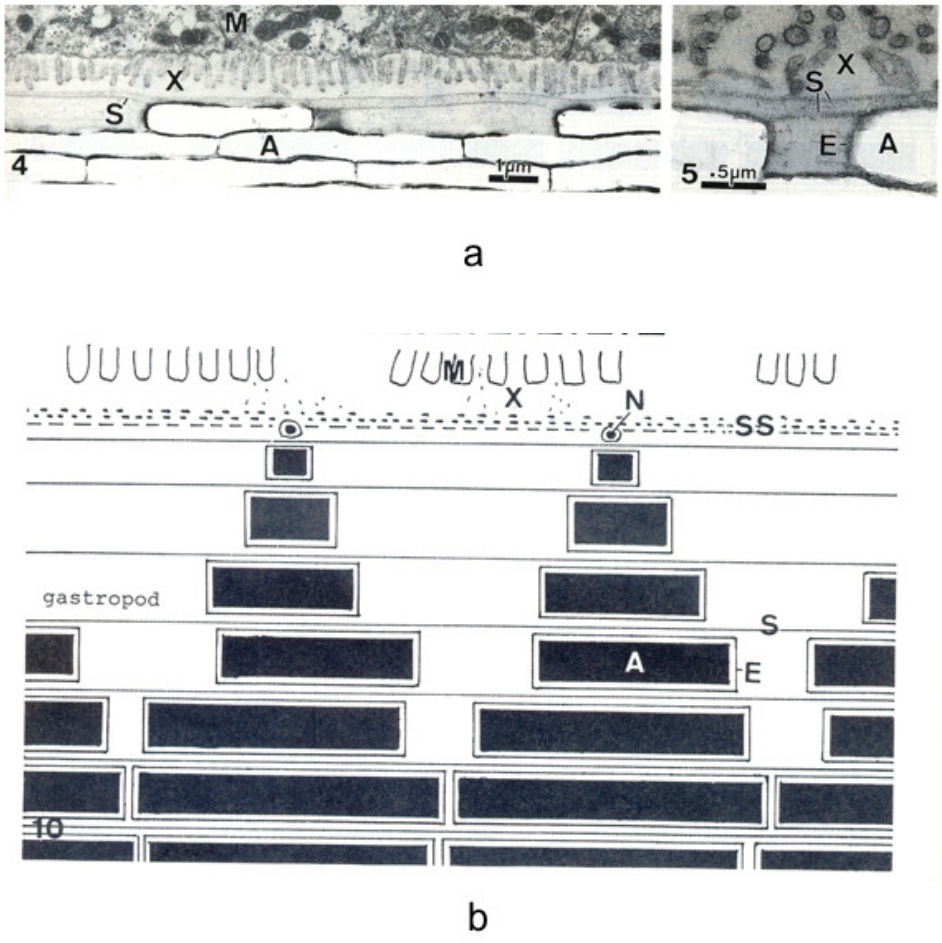

Figure 4.9: Microvilli depictions in nacre. (a) TEM of section of nacre from *Pinctada radiate*. Note the visible microvilli at the edge of the mantle epithelium (M) and extrapallial space (X). (b) Schematic illustration of nacre formation in gastropods. Aragonite tablets (A); Organic sheets (S); surface sheet (SS); Organic envelope surrounding crystals (E); Newly formed crystals (N); and part of epithelium (M) and extrapallial space (X). (*source*: Nakahara 1991)

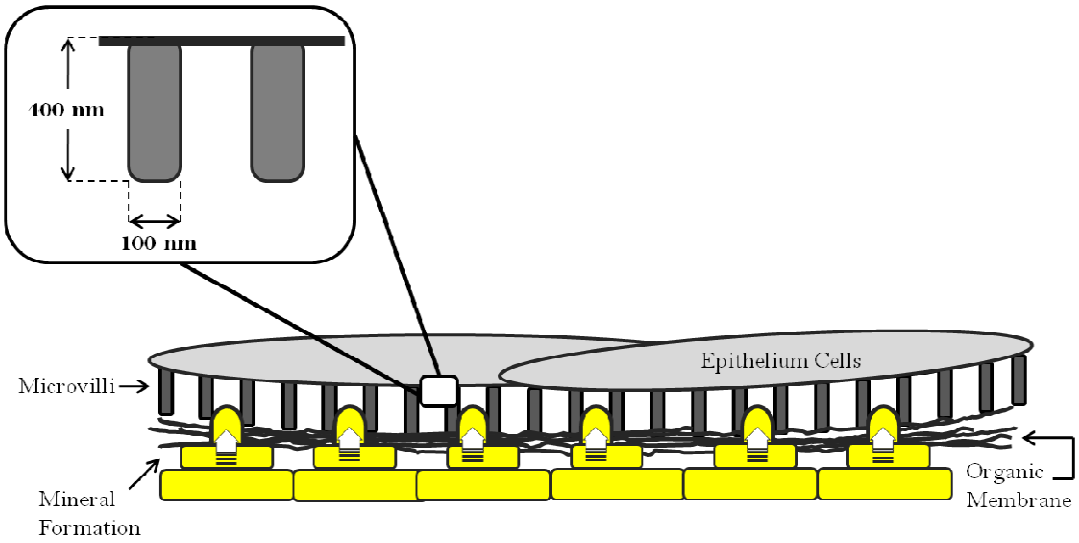

Figure 4.10: Schematic depiction of the epithelium cells containing the microvilli which are approximately 100 nm diameter and 400 nm height which involves in the deposition and position of the organic membrane.

4.3 Demineralized Shell and Organic Layer

The sectioned and demineralized shell samples from the growing edge revealed areas of thin organic intertile layer (Figure 4.12) in arrays of stretched holes. This organic intertile layer is believed to be periodically deposited (every ~0.5 μm) by the epithelium in the animal. It is composed of a thin biopolymer protein framework secreted by epithelial cells (Lowenstam and Weiner 1989). This organic layer is an important characteristic and has been studied successively (Lin et al. 2005; Meyers et al. 2008, 2009; Bezares 2008, 2010).

Lin and Meyers (Lin and Meyers 2005) investigated the thicker regions (20 μm) of organic layer that exist between the shell's mesolayers. These thick layers are believed to be formed by seasonal fluctuations where calcification is interrupted. Subsequently, Meyers et al. (Meyers et al. 2009) further noted the role of the organic

matrix (20-50 nm thick) interlayer in the formation of the $CaCO_3$ aragonite matrix into 0.5 μm thick tiles. Moreover, Meyers et al. (Meyers et al. 2009) showed further evidence of the chitin network that forms the structural component of the intertile layer and characterized it by SEM, AFM, and nanoindentation. Furthermore, Bezares et al. (Bezares 2008, 2010) described the structure of demineralized tissue and examined its mechanical response. In addition to being a key element in the excellent mechanical properties, it is also an important component in regulating the growth of the aragonite. This layer slows down the growth of the aragonite in the rapid growth (c axis) direction.

These results are in agreement with growth mechanism proposed by Meyers and coworkers (Lin et al. 2008a; Meyers et al. 2008). The growth of the mineral is allowed to proceed through the orifices in the organic layer as the transport of calcium and carbonate ions is permitted through the holes in the organic layer (Figure 4.12b). Figure 4.11 shows randomly oriented chitin macromolecule fibrils (Sarikaya 1994; Meyers et al. 2009; Checa 2009; Crenshaw et al. 1976; Weiner and Traub 1980, 1984) considered to be the structural component of the organic layer. There are two hypotheses explaining the formation and growth of the tiles: (a) Organic scaffold, into which Ca^{2+} and CO^{3-} ions penetrate, combine, and precipitate (e.g. Bezares 2008, 2010). (b) Periodic deposition of organic layer with holes, retarding the growth of aragonite crystals in the *c* direction (perpendicular to the growth surface) (Meyers et al. 2009; Lin et al. 2008b). The organic scaffold hypothesis requires intricate genetic engineering. On the other hand, the periodic chitin deposition hypothesis is directly regulated by the mantle. The results obtained by Lin et al. (Lin et al. 2008b), Meyers

et al. (Meyers et al. 2009), and here strongly support the periodic deposition hypothesis, a mechanism well described by Schäffer et al. (Schäffer et al. 1996) and Belcher et al. (Belcher et al. 1996, 1997). Especially significant is the fact that the layers between laterally adjacent tiles are much thinner than the horizontal ones (parallel to the growth surface), as shown in Figure 4.12b. Of importance also is the identification of chitin synthesis sites in the cavernous channels within the epithelium; it is proposed that they are extruded onto the growth surface by mechanical action from the abalone foot.

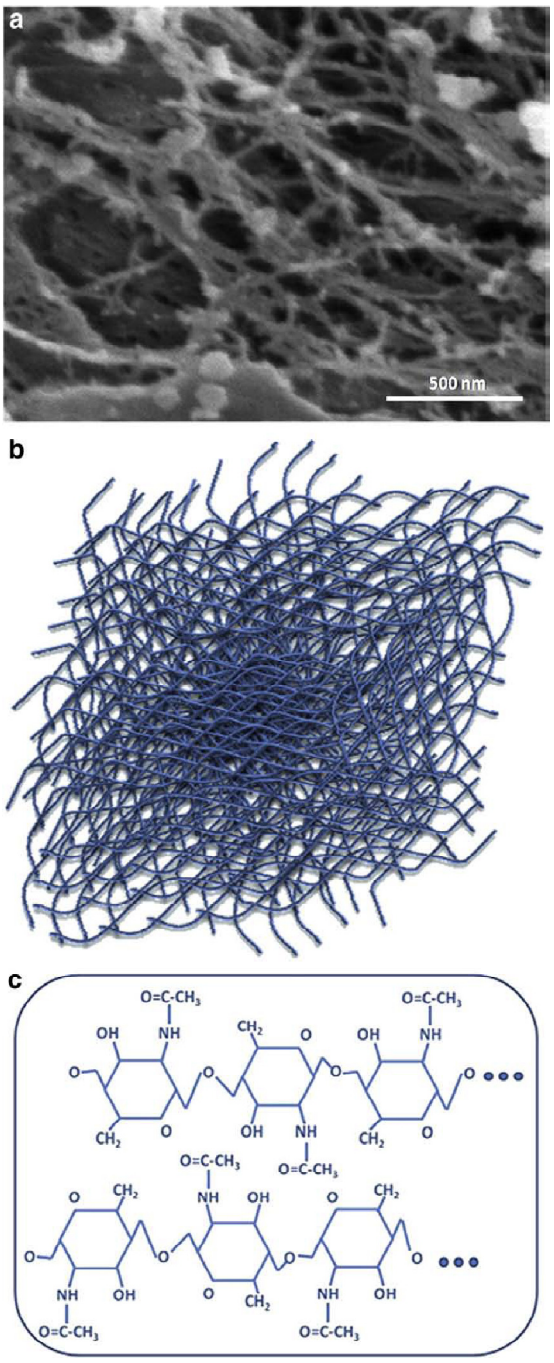

Figure 4.11: a) Demineralized shell revealing randomly oriented chitin fibrils from intertile layers; b) schematic representation of organic intertile layer composed of chitin fibrils. c) Schematic structure of chitin.

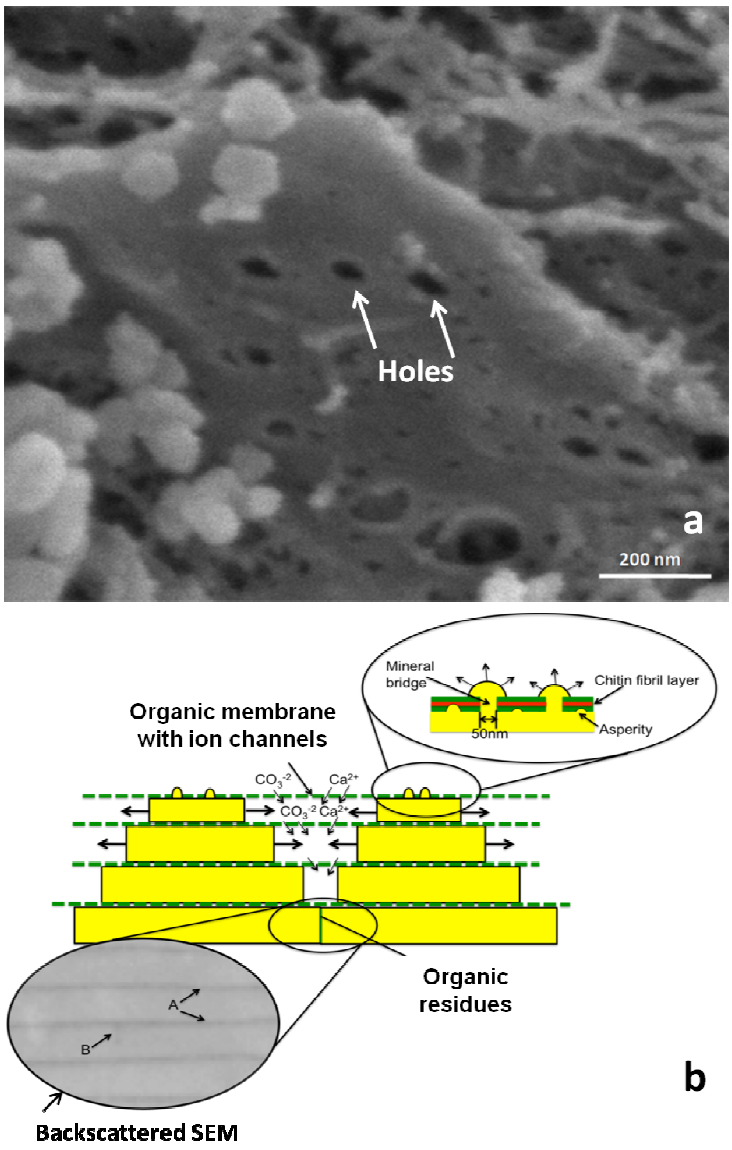

Figure 4.12: a) Thin intertile organic layer showing holes; b) Proposed Mechanism of growth of nacreous tiles by formation of mineral bridges as depicted by Meyers et al. (Meyers et al. 2009); organic layer is permeable to calcium and carbonate ions which nourish lateral growth as periodic secretion and deposition of the organic intertile membranes restricts their flux to the lateral growth surfaces. Arrows A designate organic interlayer imaged by SEM; arrow B designates lateral boundary of tile.

Figure 4.13 (a) represents the possible sequence in which growth could occur through mineral bridges. The growth sequence is as follows; (i) organic scaffolding

forms as interlamellar membranes between the layers of tiles arresting *c*-direction growth, (ii) a new tile begins growth through the porous membrane, (iii) the new tile grows in every direction, but faster along the *c*-axis, (iv) a new porous organic membrane is deposited, arresting *c*-axis growth of the new tile while allowing continued *a* and *b*-axis; growth, mineral bridges begin to protrude through the second organic membrane while sub-membrane tiles continue to grow along the *a* and *b*-axis, sub-membrane tiles abut against each other; a third tile begins to grow above the membrane.

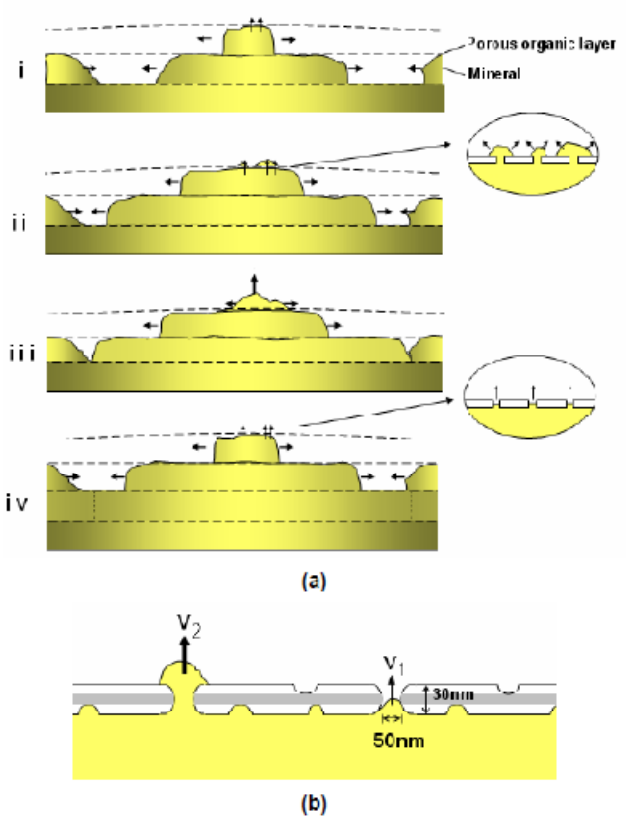

Figure 4.13: (a) Growth sequence through mineral bridges (b) Detailed view of mineral bridges forming through holes in organic membranes (*source*: Lin 2008b).

As shown, the bridges are believed to be the continuation of mineral growth in the *c*-axis from a previous layer of tiles. They protrude through the growth arresting layers of proteins, creating a site on the covering organic layer where mineralization can continue. These mineral bridges are the seed upon which the next tile forms. A schematic view of mineral bridges enabling growth through a permeable organic membrane is shown in Figure 4.12b. Holes in the organic nanolayer, which have been identified by Schäffer et al. (Schäffer et al. 1997), are thought to be the channels through which growth continues. Mineral growth above the membrane is faster than

growth in the membrane holes because of the increase in contact area with surrounding calcium and carbonate ions. Since these holes are small (30–50 nm diameter) the flow of ions is more difficult, resulting in a reduction of growth velocity to V1<<V2 (Figure 4.13b). V2 is the unimpeded growth velocity in the *c* direction.

The supply of Ca^{2+} and CO_3^{2-} ions to the growth front is enabled by their flow through the holes in the membranes. This explains why the tiles have a width-to-thickness ratio of approximately 20 whereas the growth velocity in the orthorhombic *c* direction is much higher than in the *a* and *b* direction.

Chapter 4, in part, is a reprint of the material as it appears in Lopez MI, Chen PY, McKittrick J, Meyers MA. *Materials Science and Engineering C* 2010; 31: 238-245. The thesis author was the primary investigator and author of this paper.

CHAPTER 5

SUMMARY AND CONCLUSIONS

A growth study considering seasonal changes on the mollusk *Haliotis rufescens*, commonly known as the red abalone is presented. The nacre from the shell of the abalone represents a biological composite of organic and inorganic phases which have structural hierarchies that range from the nano to the macroscale. The goal of this study is to contribute to the expanding knowledge base of biological systems serving as biomineralization models in hopes of inspiring novel techniques and designs. From these examinations, the following conclusions can be done.

The process of steady state tiled aragonite growth at different temperatures and with a variation in dieting habits is discussed in great detail. The combined utilization of the flat pearl technique and SEM observations allowed to determine that the rate of the transition from an initial random nucleation to the steady-state growth of aragonite tiles is achieved faster when the animal is kept at relatively warmer temperatures and regularly fed (21°C) than when maintained in water at colder temperatures (15 °C) or with a limitation of food (21°C).

In addition, high resolution SEM images produced evidence of an outer smooth surface and inner channels are observed in the epithelium. These channels provide a path for ion and chitin transport. The smooth outer surface is believed to mechanically flatten the growing surface of the shell. These results are comparable to previous observation by Meyers and Lin (Meyers et al. 2009; Lin et al. 2008a).

Observations of complete demineralization of abalone nacre confirmed the sheets were composed of disordered layers of cross-linked protein chains. These are sections consisting of the intertile layer composed of the chitin network. Observed and studied previously by (Lin et al. 2005; Meyers et al. 2008, 2009; Bezares 2008, 2010). This organic component is believed to influence growth mechanism of aragonite tiles by retarding, periodically, the growth in the c-axis direction. These results are strong evidence supporting the growth mechanisms proposed by Meyers et al. (Meyers et al. 2009).

It is also relevant to mention that mollusk shells are already inspiring new and better synthetic materials. In the biomedical field, it was shown that nacre can serve as a synthetic bioactive material. Nacre coatings can be transformed into apatite under mild-condition chemical methods (Vecchio et al. 2007; Guo & Zhou 2008). Thus, when nacre is integrated with bone tissue can stimulate the bone re-growth (Rousseau et al. 2008; Zhu et al. 2008). This makes it an excellent candidate for orthopaedic and dental fields.

Additionally, other attempts have been made by mimicking the nacre architecture by synthetically reproducing it by an adequate combination of inorganic crystals and organic polymers. Such as in the case of Oaki et al. (Oaki & Imai 2005; Oaki et al. 2006), which utilized the organic macromolecules as templates for the nucleation of the minerals and control of the final material's shape. Some of these have been by using a Biomimetic materials synthesis approach. This refers to utilizing methods similar to nature, either using living organisms or using the respective materials isolated from organisms to prepare inorganic products. An example of this

is work reported by Katti et al. (Katti et al. 2008), which employed the learnings of the bottom-up approach to synthesize composites of chitosan and polygalacturonic acid with hydroxyapatite by allowing precipitation of hydroxyapatite in the presence of biopolymers.

Bioinspired materials synthesis is used when concepts found in natural biomineralization are applied to the preparation of inorganic products using artificial materials. For example, a very successful approach was shown by the UC Berkeley and Lawrence Berkeley National Lab, a group led by Ritchie and Tomsia (Deville et al. 2006, Munch et al. 2008; Launey et al. 2009, 2010b) in which layered materials were prepared through a freeze-casting method; the porous scaffolds were then filled with a second phase, e.g. an organic component, in order to produce a dense composite. They combined aluminum oxide and polymethyl methacrylate (PMMA). This technique permits the formation of layered composites in various intricate shapes with outstanding mechanical properties very comparable to the structures exhibited by nacre. This similarity is observed in Figure 5.1, where the alumina tiles resemble the role of the aragonite tiles and the organic interlayer is substituted by PMMA.

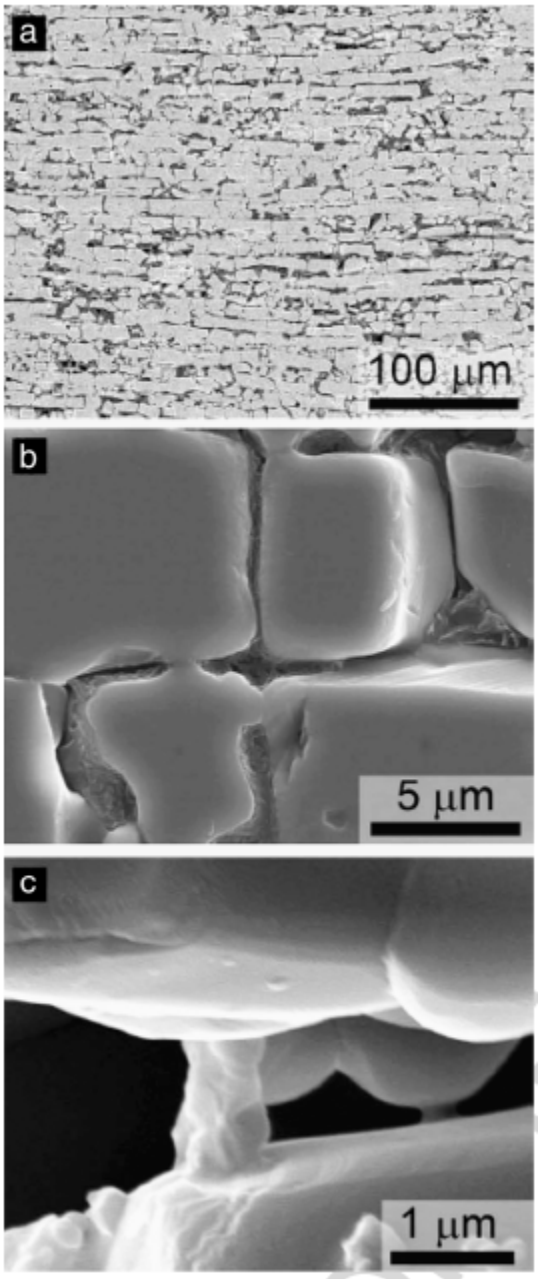

Figure 5.1: Microstructure of abalone nacre-inspired Al_2O_3/PMMA composites in (a) lamellar and (b) brick-and-mortar forms produced by freeze casting techniques; (c) bridge between two tile layers (*source*: Launey et al. 2009).

In conclusion, understanding the limited supply of materials available in biological systems and the narrow range of temperatures in which synthesis and processing takes place should aid in improving design principles of nature to amplify their effectiveness. Our current scientific and industrial capabilities can extend the biological manufacturing principles to a broader range of temperatures, pressures, and compositions, while retaining the essential features. Nature has designed and improved components and structures for 3.8 billion years, one should take this as a resource for innovation. Nature can act as a model, mentor, and measure so that these concepts can go beyond the way we design our planet, but also how we appreciate it.

REFERENCES

Arzt E. Mater Sci Eng C 2006; 26:1245-50.

Barthelat F, Li CM, Comi C, Espinosa HD. J Mater Res 2006;21:1977-1986.

Barthelat F. Phil Trans R Soc A, 2007; 365: 2907–2919.

Belcher AM, Wu XH, Christensen RJ, Hansma PK, Stucky GD, Morse DE. Nature 1996;381:56-58.

Belcher AM, Smith BL, Stucky GD, Morse DE, Hansma PK, Chem Mater, 1997; 9: 1731

Belcher AM, Gooch EE. In: *Biomineralization: from biology to biotechnology and medical application*. ed. Bauerlein E, Germany: Wiley-Interscience, 2000, p.221.

Bevelander G, Nakahara H. Calc Tiss Res 1960;7:84-92.

Bevelander G, Nakahara H. In: Omori M, Watabe N, editors. *The Mechanisms of Biomineralization in Animals and Plants*. Tokyo: Tokai University Press, 1980, pp 19-27.

Bezares J, Asaro RJ, Hawley M, J. Struct Biol, 2008; 163: 61.

Bezares J, Asaro RJ, Hawley M, J. Struct Biol, 2010; 170: 484.

Checa AG, Cartwright JHE, Willingerc MG. Proc Natl Acad Sci USA, 2009; 106: 38.

Currey JD. Proc Roy Soc Lond 1977;196: 443-463.

Currey JD. *Bones: structure and mechanics*. New Jersey: Princeton University Press, 2002.

Deville S, Saiz E, Nalla RK, Tomsia AP. Science, 2006; 311: 515.

Deville S, Saiz E, Nalla RK, Tomsia AP. Biomaterials, 2006; 27: 5480.

Erben HK. Biomineral 1972;4:15-27.

Erben HK, Watabe N. Nature 1974; 248:128.

Espinosa HD, Rim JE, Barthelat F, Buehler M, Prog Mater Sci, 2009; 54: 1059.

Evans AG, Suo Z, Wang RZ, Aksay IA, He MY, Hutchinson JW. J Mater Res Soc 2001;16:2475.

Fratzl P. J. R. Soc. Interface, 2007; 4: 637–642.

Fratzl, P and Weinkamer R. Prog Mater Sci, 2007; 52: 1263–1334

Fritz M, Belcher AM, Radmacher M, Walters DA, Hansma PK, Strucky GD, and Morse DE. Nature 1994 ;371: 49.

Fritz M, Morse DE. Col Int Sci 1998;3:55.

Gao HJ, Ji BH, Jäger IL, Arzt E, Fratzl P. Proc Natl Acad Sci USA 2003;100:5597-5600.

Gao HJ, Wang X, Yao H, Gorb S, Arzt E. Mechanics of Mater 2005;37:275 -286.

Heiland B, Schneider AS, Arzt E, and Weiss IM, Schalen, Report, INM – Leibniz Institut für Neue Materialien, Saarbrücken, 2011

Jackson AP, Vincent JFV, Turner RM. Proc Roy Soc Lond B 1988;B234:415.

Ji BH, Gao HJ. J Mech Phy Solid 2004;52:1963-1990.

Ji BH, Gao HJ, Hsia KJ. Phil Mag Lett 2004;84:631-641.

Katti, KS & Katti DR, Mater. Sci. Eng. C, 2006; 26: 1317–1324.

Katti, KS & Katti DR, Bhosle A, Pradhan S. J. Mater Res, 2005; 20: 1097–1100.

Kobayashi I and Samata T. Mater. Sci. Eng. C 2006; 26: 692–698.

Lapota D, Rosen G, Chock J, Liu CH. J Shellfish Res 2000;19:431.

Launey ME, Munch E, Alsem DH, Barth HB, Saiz E, Tomsia AP, Ritchie RO. Acta Mater.,
2009; 57: 2919.

Levi-Kalisman Y, Falini G, Addadi L, Weiner S. J. Struct Biol, 2001; 135: 8–17.

Lin AYM, Meyers MA, Mater. Sci. Eng. A, 2005; 390: 27.

Lin AYM, Meyers MA, Vecchio KS. Materials Science and Engineering C 2006;16:1370-1389.

Lin AYM, Chen PY, Meyers MA. Acta Biomaterialia 2008;4:131-138.

Lin AYM, Ph.D. Thesis, University of California, San Diego, 2008.

Luz GM and Mano JF. Phil. Trans. R. Soc. A 2009; 367: 1587-1605

Manne S and Aksay A. Curr Opin Solid State Mater Sci, 1997; 2: 358–364.

Mayer G, Sarikaya M. Exper Mech 2002;42:395.

Mayer G. Science 2005; 310: 1144.

Menig R, Meyers MH, Meyers MA, Vecchio KS. Acta Mater 2000;48:2383-2398.

Meyers MA, Lin AYM, Chen PY, Muyco J. J Mech Beh. Biolog Mater 2008; 1:76-85.

Meyers MA, Lim CT, Li A, Hairul Nizam BR, Tan EPS, Seki Y, McKittrick J. Mat.Sci. Eng. C., 2009; 29: 2398.

Meyers MA, Chen PY, Lopez ML, Seki Y, Lin AY. J Mech Beh. Biomed Mater in press, 2011.

Munch E, Launey ME, Alsem DH, Saiz E, Tomsia AP, Ritchie RO. Science, 2008; 322: 1516.

Mutvei H, in: M. Omori, N. Watabe (Eds.), The Mechanisms of Biomineralization in Animals and Plants, Tokai Univ. Press, 1980, p. 49.

Nakahara H. Venus, 1979; 38: 205.

Nakahara H. Calcification of Gastropod Nacre. In: *Biomineralization and Biological Metal Accumulation.* ed. Westbroek P, De Jong EW. Dordrecht, Holland: D. Reidel Publishing Company, 1982, pp 225.

Nakahara H, Bevelander G, Kakei M. Venus Jpn J Malac 1982; 41:33-46.

Nakahara H. Nacre Formation in Bivalve and Gastropod Molluscs. In: *Mechanisms and Phylogeny of Mineralizaion in Biological Systems*. ed. Suga S, Nakahara H. New York: Springer-Verlag,1991, pp 343.

Nudelman F, Gotliv BA, Addadi L, Weiner S. J Struct Biol 2006;153:176-187.

Sanchez C, Arribart H, Giraud-Guille MM. Nat. Mater. 2005; 4: 277.

Sarikaya M, Gunnison KE, Yasrebi M, Aksay JA. Mater Res Soc 1990;174:109.

Sarikaya M, Aksay JA. In: *Results and Problems in Cell Differentiation in Biopolymers*. Case S. ed., Springer Verlag, Amsterdam, 1992 p.1.

Sarikaya M. Microscopy research and technique 1994; 27:360.

Schäffer TE, Ionescu-Zanetti C, Proksch R, Fritz M, Walters DE, Almqvist N, Zaremba CM, Belcher AM, Smith BL, Stucky GD, Morse DE, Hansma PK. Chem Mater 1997;9:1731-1740.

Shen XY, Belcher AM, Hansma PK, Stucky GD, Morse DE. J. Bio Chem; 1997; 272: 32472-81.

Simkiss K, Wilbur KM. *Biomineralization*, Academic Press, 1989.

Smith BL, Schäffer TE, Viani M, Thompson JB, Frederick NA, Kindt J, Belcher AM, Stucky GD, Morse DE, Hansma PK, Nature, 1999; 399: 761–763.

Song F, Zhang XH, Bai YL. J Mater Res 2002;17:1567–70.

Song F, Soh AK, Bai YL. Biomaterials 2003;24:3623.

Srinivasan AV, Haritos GK, Hedberg FL. App Mech Rev 1991;44:463.

Su XW, Belcher AM, Zaremba CM, Morse DE, Stucky GD, Heuer AH. Chem Mater 2002;14:3106-3117.

Sumitomo T, Kakisawa H, Owaki Y, Kagawa Y. J. Mater. Res. 2008; 23: 1466–1471.

Thompson DW. *On growth and form.* 2nd ed., reprinted Cambridge: Cambridge University Press, 1968.

Vincent JFV. *Structural biomaterials*. Revised ed. New Jersey: Princeton Universtiy Press,1991.
Velazquez-Castillo RR, Reyes-Gasga J, Garcia-Gutierrez DI, Yacaman MJ. Biomaterials, 2006; 27: 4508-4517

Wada, K. Bull Japanese Soc Sci Fish 1958; 24:421-427

Wada, K. Bull Japanese Soc Sci Fish 1959;25:342-345.

Wada K. Biomineralization, 1972; 6: 84

Wang CA, Long B, Lin W, Huang Y, Sun J. J. Mater Res, 2008; 23: 1706–1712.

Watabe N, Wilbur KM. Nature 1960;188:334

Weibull W. J Appl Mech 1951;18:293.

Wise SW. Science 1970;167:1486-88.

Zaremba CM, Belcher AM, Fritz M, Li Y, Mann S, Hansma PK, and Morse DE. Chem Mater 1996;8:679.

Zhang S, Marini DM, Hwang W, Santoso S. Current Opinion in Chemical Biology 2002; 6:865-871.